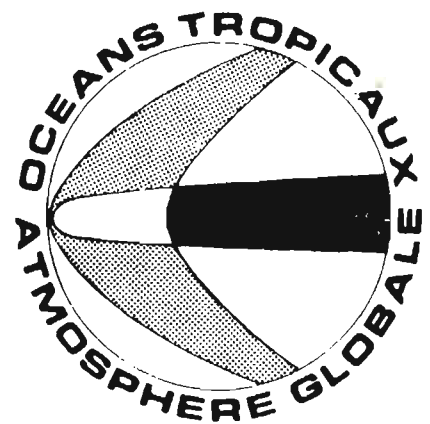# Influence of density structure and bottom depth on vertical modal calculation in the Tropical Pacific Ocean

Influence de la structure de densité et de la profondeur du fond sur les calculs de modes verticaux dans l'Océan Pacifique Tropical

Laurence SOMBARDIER

Stage effectué du 20 janvier au 6 juin 1989

au Centre ORSTOM de Nouméa

OCÉANS TROPICAUX ATMOSPHERE GLOBALE

INSTITUT FRANÇAIS DE RECHERCHE SCIENTIFIQUE
POUR LE DÉVELOPPEMENT EN COOPÉRATION

ORSTOM

Centre de Nouméa

1989

Influence of ·density structure and bottom depth on vertical modal calculation in the Tropical Pacific Ocean

Influence de la structure de densité et de la profondeur du fond sur les calculs de modes verticaux dans l'Océan Pacifique Tropical

Laurence SOMBARDIER

ABSTRACT

Vertical modal calculations were performed on a one degree longitude-latitude grid over the tropical Pacific using the Levitus salinity and temperature file and a bathymetry file. To observe the influence of density structure and bottom depth, the calculations were also made with a flat bottom as well as with a mean density structure. Density is found far a more important parameter than bottom depth for modal calculations. Close examination of modal structures at depth with a more precise NODC CTD file showed that it is crucial to know the density profile for the first 500 meters in order to obtain meaningful modal values.

RESUME

Une décomposition en modes verticaux a été effectuée sur une grille longitude-latitude sur tout le Pacifique Tropical à partir du fichier Levitus de température et de salinité et d'un fichier bathymétrique. Afin d'estimer l'influence de la structure de densité et de la profondeur, les calculs ont été aussi effectués avec un fond plat et avec une densité moyenne. La densité est ainsi apparue comme un paramètre beaucoup plus important que la profondeur pour les calculs de décomposition modale. L'examen détaillé des structures modales à différentes profondeur, grâce à un fichier NODC sonde CTD beaucoup plus précis, a montré qu'il était crucial de connaitre le profil de densité sur les premiers 500m, afin d'obtenir une décomposition modale significative.

REMERCIEMENTS

CONTENTS

I INTRODUCTION

Vertical and horizontal modal decompositions have been widely used in theoretical models of equatorial dynamics. A quick survey of the models developed is provided by McCreary (1985). Thus, modal decomposition, as a mathematical tool, is primordial.

For example, the most successful models for El Nino describe the onset of the phenomenon, after the trade wind collapse in the western Pacific, in terms of equatorially trapped waves.

In the past years, oceanographers have been interested in finding if the modal structures have any physical reality. The resolution of the vertical modes with observational data has been successful in several cases. For example, Hayes et al., (1985) have looked into the problem and developed a technique to study the expected errors of a modal expansion using observational data. Toole and Borges (1984) discussed CTD data, collected from the R.V. Conrad in the early stages of the 1982/1983 El Nino, in terms of trapped waves and showed the existence of Kelvin waves. Behringer (1984) fitted, with relative success, dynamical modes to data originating from CTD casts. Modal fits to near equatorial data at 85°W in 1982 were also performed by Toole (1985). Tang et al. (1988) also showed evidence of vertical modes in the Eastern Equatorial Pacific Ocean.

Hence, one can consider that vertical modal decomposition have a physical relevance. Therefore, one can expect that modal calculations will be performed regularly in the future. The purpose of this report is to examine the influence of bottom depth and density structure on these calculations. And since information at depth is not always readily available, we would also like to find out how much information is really necessary to calculate correct modal structures.

II THEORETICAL REVIEW

A perturbation from a rest state of an homogeneous inviscid fluid (i.e. uniform density) will generate a disturbance of the surface which can take the form of a horizontal traveling wave or standing wave. In reality, the ocean is continuously stratified since temperature, salinity and pressure are not constant parameters within the world oceans. One can imagine an ocean with a two layer configuration (the two layers having different densities and being immiscible). The treatment of such a problem, which was first performed by Stokes in 1947 (Gill, 1982), gives a simplified idea of the effects of stratification. A perturbation in such a system will generate an internal oscillation at the interface of the two layers.

A continuously stratified fluid corresponds to a fluid with an infinite amount of layers. These layers can be considered as extremely thin sheets of fluid since the horizontal scale of the ocean is much larger than the vertical scale. Thus, one can use the technique of separation of variables when examining the equations of motion of the system. The solution can then be expressed as a sum of normal modes. A normal mode has a fixed vertical structure and behaves in the horizontal dimension and in time in the same way as does a homogeneous fluid with free surface (Gill, 1982). The next four sections will provide a brief theoretical review of modal decomposition.

A. The Governing Equations

Considering a continuously stratified ocean, the equation of motion, in its most general form, is given by:

$$\rho \frac{d\vec{v}}{dt} + 2\rho \vec{\Omega} \times \vec{v} = -\vec{\nabla}P + \rho \vec{g} + \mu \nabla^2 \vec{v} + \vec{F}$$

where
- ρ is density
- $\vec{g}$ is gravity
- $\vec{\Omega}$ is earth's rotation
- μ is the viscosity coefficient
- $\vec{\nabla}P$ is the pressure gradient
- $\vec{F}$ is the resultant of the other external forces acting on a fluid particle
- ∇^2 is the Laplacian

$$\frac{d}{dt} = \frac{\partial}{\partial t} + \vec{v}.\vec{\nabla} \quad \text{is the total time derivative}$$

The other important governing equation is the mass conservation equation:

$$\frac{d\rho}{dt} + \rho \vec{\nabla}.\vec{v} = 0$$

Several assumptions need to be made in order to obtain workable equations. The first assumption is that we are dealing with an incompressible fluid. Thus, $\vec{\nabla}.\vec{v} = 0$. We shall also assume that the fluid is ideal, i.e. $\mu = 0$. F is taken to be null (there are no external forces besides gravity acting on the fluid particles). The horizontal components of earth's rotation are also neglected. Thus, $\Omega_x = \Omega_y = 0$. If the disturbances due to internal waves have small amplitudes, the non-linear convective terms ($(\vec{v}\vec{\nabla})\vec{v}$) may be neglected. This approximation, called linearization, is crucial because it allows to solve the wave equation by normal modes.

Hence, after these approximations, the governing equations of motion become:

$$\rho \frac{\partial u}{\partial t} - \rho f v + \frac{\partial P}{\partial x} = 0$$

$$\rho \frac{\partial v}{\partial t} + \rho f u + \frac{\partial P}{\partial y} = 0$$

$$\rho \frac{\partial w}{\partial t} + \frac{\partial P}{\partial z} - \rho g = 0$$

f is the Coriolis parameter defined by:

$$f = 2\Omega_z = 2\omega \sin\phi$$

We also have the continuity equation:

$$\frac{\partial u}{\partial x} + \frac{\partial v}{\partial y} + \frac{\partial w}{\partial z} = 0$$

One more assumption is necessary: the Boussinesq approximation. Let us define : ρ and P as a sum of a background state $\rho_0(z)$ and $P_0(z)$, and fluctuations $\rho'(x,y,z,t)$ and $P'(x,y,z,t)$ due to internal waves :

$$\rho = \rho o\,(z) + \rho'\,(x,y,z,t)$$

$$P = P_0(z) + P'(x,y,z,t)$$

$$\frac{d\rho_o}{dz} - \rho_o\, g = 0 \qquad \text{Hydrostatic equilibrium}$$

If the fluctuation amplitudes are small, ρ_0 will be much larger than ρ' and P_0 will be much larger than P'. Also, $\partial \rho/\partial t$ will be significantly greater than $\vec{v} \cdot \vec{\nabla}\rho'$. The boussinesq approximation consists in neglecting ρ' as far as inertia terms are concerned but taking density variations in full account as far as buoyancy forces are concerned (Gill, 1982). Hence, ρ cannot be neglected in the term containing g.

Thus, the final equations are:

(1)
$$\rho_o\, \frac{\partial u}{\partial t} - \rho_o\, f v + \frac{\partial P'}{\partial x} = 0$$

(2)
$$\rho_o\, \frac{\partial v}{\partial t} + \rho_o\, f u + \frac{\partial P'}{\partial y} = 0$$

(3)
$$\rho_o\, \frac{\partial w}{\partial t} + \frac{\partial P'}{\partial z} - g \rho' = 0$$

(4)
$$\frac{\partial \rho'}{\partial t} + w\, \frac{\partial \rho_o}{\partial z} = 0$$

B. The Vertical Structure of Internal Waves

1. *The Vertical Velocity Equation*

The vertical velocity equation is obtained by eliminating progressively p', ρ', u and v from the governing equations. Roberts (1975) method shall be used. We shall derive equation (1) with respect to z and substract it from equation (3) derived with respect to x. Similarly, we shall derive equation (2) with respect to z and substract it from equation (3) derived with respect to y.

$$\frac{\partial(3)}{\partial x} - \frac{\partial(1)}{\partial z} = \frac{\partial \rho_0}{\partial x}\frac{\partial w}{\partial t} + \rho_0 \frac{\partial^2 w}{\partial x \partial t} + \frac{\partial^2 P'}{\partial x \partial z} - g\frac{\partial \rho'}{\partial x} - \frac{\partial \rho_0}{\partial x}\frac{\partial u}{\partial t}$$

$$- \rho_0 \frac{\partial^2 u}{\partial t \partial z} + \rho_0 F \frac{\partial v}{\partial z} + \frac{\partial \rho_0}{\partial z} f v - \frac{\partial^2 P'}{\partial z \partial x}$$

$$\frac{\partial(3)}{\partial y} - \frac{\partial(2)}{\partial z} = \frac{\partial \rho_0}{\partial y}\frac{\partial w}{\partial t} + \rho_0 \frac{\partial^2 w}{\partial t \partial y} + \frac{\partial^2 P'}{\partial y \partial z} - g\frac{\partial \rho'}{\partial y} - \frac{\partial \rho_0}{\partial z}\frac{\partial v}{\partial t}$$

$$- \rho_0 \frac{\partial^2 v}{\partial z \partial t} - \frac{\partial \rho_0}{\partial z} F u - \rho_0 F \frac{\partial u}{\partial z} - \frac{\partial^2 P'}{\partial z \partial y}$$

Adding the two equations obtained and simplifying with $\frac{d \rho_0}{d z} = 0$, we have:

$$-\frac{\partial}{\partial t}\left(\frac{\partial u}{\partial z} + \frac{\partial v}{\partial z}\right) + \frac{\partial}{\partial t}\left(\frac{\partial w}{\partial x} + \frac{\partial w}{\partial y}\right) + F\left(\frac{\partial v}{\partial z} - \frac{\partial u}{\partial z}\right) - \frac{g}{\rho_0}\left(\frac{\partial \rho'}{\partial x} + \frac{\partial \rho'}{\partial y}\right) = 0$$

Deriving this expression with respect to t:

$$\frac{\partial^2}{\partial t^2}\left(\frac{\partial u}{\partial z} + \frac{\partial v}{\partial z}\right) - \frac{\partial^2}{\partial t^2}\left(\frac{\partial w}{\partial x} + \frac{\partial w}{\partial y}\right) - F\frac{\partial}{\partial t}\left(\frac{\partial v}{\partial z} - \frac{\partial u}{\partial z}\right)$$

$$+ \frac{g}{\rho_0}\left(\frac{\partial^2 \rho'}{\partial t \partial x} + \frac{\partial^2 \rho'}{\partial t \partial y}\right) = 0$$

But, from equation (4), $\quad \frac{\partial \rho'}{\partial t} = -w\frac{\partial \rho_0}{\partial z}$

Hence, $\quad \frac{g}{\rho_0}\left(\frac{\partial^2 \rho'}{\partial t \partial x} + \frac{\partial^2 \rho'}{\partial t \partial y}\right) = -\frac{g}{\rho_0}\frac{\partial \rho_0}{\partial z}\left(\frac{\partial w}{\partial x} + \frac{\partial w}{\partial y}\right) = 0$

Differenciating with respect to x and y:

$$\frac{\partial^2}{\partial t^2}\frac{\partial}{\partial x}\left(\frac{\partial u}{\partial z} + \frac{\partial v}{\partial z}\right) - \frac{\partial^2}{\partial t^2}\frac{\partial}{\partial x}\left(\frac{\partial w}{\partial x} + \frac{\partial w}{\partial y}\right) - F\frac{\partial^2}{\partial t \partial x}\left(\frac{\partial v}{\partial z} - \frac{\partial u}{\partial z}\right) - \frac{g}{\rho_0}\frac{d\rho_0}{dz}\frac{\partial}{\partial x}\left(\frac{\partial w}{\partial x} + \frac{\partial w}{\partial y}\right) = 0$$

$$\frac{\partial^2}{\partial t^2}\frac{\partial}{\partial y}\left(\frac{\partial u}{\partial z} + \frac{\partial v}{\partial z}\right) - \frac{\partial^2}{\partial t^2}\frac{\partial}{\partial y}\left(\frac{\partial w}{\partial x} + \frac{\partial w}{\partial y}\right) - F\frac{\partial^2}{\partial t \partial y}\left(\frac{\partial v}{\partial z} - \frac{\partial u}{\partial z}\right) - \frac{g}{\rho_0}\frac{d\rho_0}{dz}\frac{\partial}{\partial y}\left(\frac{\partial w}{\partial x} + \frac{\partial w}{\partial y}\right) = 0$$

Adding these two expressions together:

$$\frac{\partial^2}{\partial t}\left[\frac{\partial}{\partial z}\left(\frac{\partial u}{\partial x}+\frac{\partial v}{\partial y}\right)\right]-\frac{\partial^2}{\partial t^2}\left[\frac{\partial^2 w}{\partial x^2}+\frac{\partial^2 w}{\partial y^2}\right]+\frac{\partial^2}{\partial t^2}\left[\frac{\partial}{\partial y}\left(\frac{\partial u}{\partial z}-\frac{\partial w}{\partial x}\right)+\right.$$

$$\left.\frac{\partial}{\partial x}\left(\frac{\partial v}{\partial z}-\frac{\partial w}{\partial y}\right)\right]-\frac{g}{\rho_o}\frac{d\rho_o}{dz}\left(\frac{\partial^2 w}{\partial x^2}+\frac{\partial^2 w}{\partial y^2}\right)-\frac{g}{\rho_o}\frac{d\rho_o}{dz}\left(2\frac{\partial^2 w}{\partial x\partial y}\right)$$

$$-F\frac{\partial^2}{\partial x\partial t}\left(\frac{\partial v}{\partial x}-\frac{\partial u}{\partial y}\right)-F\frac{\partial^2}{\partial z\partial t}\left(\frac{\partial v}{\partial y}-\frac{\partial u}{\partial x}\right)=0$$

The equation is simplified to the following:

$$\frac{\partial^2}{\partial t^2}\left[\frac{\partial}{\partial z}\left(\frac{\partial u}{\partial x}+\frac{\partial v}{\partial y}\right)\right]-\frac{\partial^2}{\partial t^2}\left(\frac{\partial^2 w}{\partial x^2}+\frac{\partial^2 w}{\partial y^2}\right)-\frac{g}{\rho_o}\frac{d\rho_o}{dz}\left(\frac{\partial w}{\partial x^2}+\frac{\partial w}{\partial y^2}\right)$$

$$-F\frac{\partial^2}{\partial t\partial z}\left(\frac{\partial v}{\partial x}-\frac{\partial u}{\partial y}\right)\simeq 0$$

From the continuity equation, we have:

$$\frac{\partial u}{\partial x}+\frac{\partial v}{\partial y}+\frac{\partial w}{\partial z}=0\quad\Longrightarrow\quad -\frac{\partial w}{\partial z}=\frac{\partial u}{\partial x}+\frac{\partial v}{\partial y}$$

Thus,

$$-\frac{\partial^2}{\partial t^2}\left(\frac{\partial^2 w}{\partial z^2}\right)-\frac{\partial^2}{\partial t^2}\left(\frac{\partial^2 w}{\partial x^2}+\frac{\partial^2 w}{\partial y^2}\right)-\frac{g}{\rho_o}\frac{d\rho_o}{dz}\left(\frac{\partial^2 w}{\partial x^2}+\frac{\partial^2 w}{\partial y^2}\right)-F\frac{\partial^2}{\partial z\partial t}\left(\frac{\partial v}{\partial x}-\frac{\partial u}{\partial y}\right)=0$$

But,

$$-\frac{d^2}{dt^2}\left(\frac{\partial^2 w}{\partial z^2}+\frac{\partial^2 w}{\partial x^2}+\frac{\partial^2 w}{\partial y^2}\right)=-\frac{\partial^2}{\partial t^2}\nabla^2 w$$

We also have:

$$0=\frac{\partial 1}{\partial y}-\frac{\partial 2}{\partial x}=\rho_o\frac{\partial^2 u}{\partial t\partial y}-\rho_o F\frac{\partial v}{\partial y}+\frac{\partial^2 P'}{\partial x\partial y}-\rho_o\frac{\partial^2 v}{\partial t\partial x}-\rho_o F\frac{\partial u}{\partial x}-\frac{\partial^2 P'}{\partial x\partial y}$$

$$\Longrightarrow\quad \frac{\partial}{\partial t}\left(\frac{\partial u}{\partial y}-\frac{\partial v}{\partial x}\right)-F\left(\frac{\partial v}{\partial y}+\frac{\partial u}{\partial x}\right)=0$$

$$\Longrightarrow\quad \frac{\partial}{\partial t}\left(\frac{\partial v}{\partial x}-\frac{\partial u}{\partial y}\right)=-F\frac{\partial w}{\partial z}$$

Therefore,

$$-\frac{\partial^2}{\partial t^2}\nabla^2 w-\frac{g}{\rho_o}\frac{d\rho_o}{dz}\left(\frac{\partial^2 w}{\partial x^2}+\frac{\partial^2 w}{\partial y^2}\right)-F\frac{\partial}{\partial z}\left(-F\frac{\partial w}{\partial z}\right)=0$$

Let

$$\nabla_H^2=\frac{\partial^2}{\partial x^2}+\frac{\partial^2}{\partial y^2}$$

and

$$N=\left(\frac{g}{\rho_o}\frac{d\rho_o}{dz}\right)^{1/2},\quad\text{Brunt-Vaisala frequency}$$

Thus,

$$\frac{\partial^2}{\partial t^2}\nabla^2 w+N^2\nabla_H^2 w+F^2\frac{\partial w}{\partial z^2}=0$$

This is the vertical velocity equation.

2. Vaisala Frequency

Consider a fluid particle displaced vertically through a small disturbance ξ from its equilibrium position without disturbing the fluid's stratification and then released. It's motion can be described by the following equations:

$$\rho_0 \frac{\partial w}{\partial t} + \frac{\partial p'}{\partial z} - g\rho' = 0$$

$$\frac{\partial \rho'}{\partial t} + w \frac{d\rho_0}{dz} = 0$$

By definition, $\omega = \frac{d\xi}{dt}$. Thus,

$$\frac{\partial \rho'}{\partial t} + \frac{\partial \xi}{\partial t} \frac{\partial \rho_0}{dz} = 0 \Rightarrow \rho' = -\xi \frac{d\rho_0}{dz}$$

Replacing ρ' in the first expression, we obtain:

$$\rho_0 \frac{\partial^2 \xi}{\partial t^2} + g\xi \frac{\partial \rho_0}{dz} - \frac{\partial \xi}{\partial z} \frac{d\rho_0}{dz} - \xi \frac{d^2\rho_0}{dz^2} = 0$$

The last two terms may be neglected. Hence,

$$\frac{\partial^2 \xi}{\partial t^2} + \frac{g}{\rho_0} \xi \frac{d\rho_0}{dz} = 0$$

$$\Rightarrow \frac{\partial^2 \xi}{\partial t^2} + N^2 \xi = 0 \qquad with \qquad N^2 = \frac{g}{\rho_0} \frac{d\rho_0}{dz}$$

Stability occurs if $\frac{d\rho_0}{dz} > 0$, i.e., $N^2 > 0$

The fluid particle, displaced from its equilibrium position, will oscillate around it in a simple harmonic motion whose frequency is N, called Vaisala frequency (or Brunt-Vaisala frequency). N is the natural frequency of oscillation for a fluid particle in a stratified ocean. The corresponding period $2\pi/N$ varies from a few minutes in the thermocline, where the density gradient is high, to a few hours in the deep ocean.

3. Solution to the Vertical Velocity Equation

We are looking for a solution to the vertical velocity equation which has the form of:

$$w = W(z)\, e^{i(k_x x + k_y y - \sigma t)} \qquad k_H = \sqrt{k_x^2 + k_y^2}$$

Applying this to the governing equation, we obtain:

$$\frac{\partial^2}{\partial t^2} \left\{ e^{i(k_x x + k_y y - \sigma t)} \left[W(z)(k_x^2 + k_y^2) + \frac{\partial^2 W(z)}{\partial z^2} \right] \right\}$$

$$+ N^2 e^{i(k_x x + k_y y - \sigma t)} W(z) [k_x^2 + k_y^2)$$

$$+ \sigma^2 \frac{d^2 W}{dz^2} e^{i(k_x x + k_y y - \sigma t)} = 0$$

$$\Rightarrow \frac{d^2 W}{dz^2} + R^2(z)\, k_H W = 0$$

where $\quad R^2(z) = \dfrac{N^2 - \sigma^2}{\sigma^2 - f^2}$

Limiting to cases when $\sigma > f$:

-If $N < \sigma$: $W(z)$ is a monotonous function of z. The only possible mode is a surface wave which is maximum at the surface and disappears at depth.

-If $N > \sigma$: $W(z)$ is an oscillatory function which changes sign in the depth interval where $N > \sigma$. An infinity of solutions are possible for an infinity of discrete values of k_H .

4. *Boundary Conditions*

BOTTOM BOUNDARY CONDITIONS

For an ideal fluid, the velocity at the bottom should be tangent to it. For a viscous fluid, the velocity should be zero at the fixed boundary. If $z=H(x,y)$ is the bottom function, then $w = u\dfrac{\partial H}{\partial x} + v\dfrac{\partial H}{\partial y}$ at $z = H(x,y)$. For a horizontal bottom, $H=$ constant and Thus, $w=0$ at $z=H$.

FREE SURFACE CONDITION

At the surface, the variation of the pressure of the fluid is equal to the atmospheric pressure ($P_a(x,y,t)$). Thus, $\quad \dfrac{\partial P}{\partial t} = \dfrac{\partial P_a}{\partial t}$

But, $\quad \dfrac{\partial P}{\partial t} \simeq \dfrac{\partial P'}{\partial t} + w\dfrac{\partial P_0}{\partial z} = \dfrac{\partial P'}{\partial t} + \rho_0 g w \simeq \dfrac{\partial P_a}{\partial t}$

If we suppose that P_a is constant, we have:

$$\dfrac{\partial P'}{\partial t} = -\rho_0 g w$$

Deriving respectively (1), (2) and (3) with respect to x, y and z and adding them together, we obtain:

$$\rho_0 \dfrac{\partial^2 u}{\partial t \partial x} - \rho_0 F \dfrac{\partial v}{\partial x} + \dfrac{\partial^2 P'}{\partial x^2} + \rho_0 \dfrac{\partial^2 v}{\partial t \partial y} + \rho_0 F \dfrac{\partial u}{\partial y} + \dfrac{\partial^2 P'}{\partial y^2} + \rho_0 \dfrac{\partial^2 w}{\partial t \partial z}$$

$$+ \dfrac{\partial^2 P'}{\partial z^2} - g\dfrac{\partial P'}{\partial z} = 0$$

$$\Rightarrow \rho_0 \dfrac{\partial}{\partial t}\left(\dfrac{\partial u}{\partial x} + \dfrac{\partial v}{\partial y} + \dfrac{\partial w}{\partial z}\right) + \dfrac{\partial}{\partial z}\left(\dfrac{\partial P'}{\partial z} - g P'\right) + \nabla_H^2 P'$$

$$+ \rho_0 F\left(\dfrac{\partial u}{\partial y} - \dfrac{\partial v}{\partial x}\right) = 0$$

From equation (3):

$$\rho_0 \dfrac{\partial w}{\partial t} = -\left(\dfrac{\partial P'}{\partial z} - g P'\right)$$

Thus, using the continuity equation, we get:

$$\rho_0 \dfrac{\partial^2 w}{\partial z \partial t} - \nabla_H^2 P' - \rho_0 F\left(\dfrac{\partial u}{\partial y} - \dfrac{\partial v}{\partial x}\right) = 0$$

Deriving with respect to t:

$$\rho_o \frac{\partial^3 w}{\partial z \partial t^2} - \frac{\partial}{\partial t}(\nabla_H^2 P') - \rho_o F \frac{\partial}{\partial t}\left(\frac{\partial u}{\partial y} - \frac{\partial v}{\partial x}\right) = 0$$

Earlier, we have derived that:

$$\frac{\partial}{\partial t}\left(\frac{\partial v}{\partial x} - \frac{\partial u}{\partial y}\right) = -F\left(\frac{\partial u}{\partial x} + \frac{\partial v}{\partial y}\right) = F\frac{\partial w}{\partial z}$$

Hence,

$$\rho_o \frac{\partial^3 w}{\partial z \partial t^2} - \nabla_H^2\left(\frac{\partial P'}{\partial t}\right) + \rho_o F^2 \frac{\partial w}{\partial z} = 0$$

Applying $\frac{\partial P'}{\partial t} = -\rho_o g w$, we obtain:

$$\rho_o\left\{\frac{\partial^2 w}{\partial z \partial t} + g \nabla_H^2 w + F^2 \frac{\partial w}{\partial z}\right\} = 0$$

$$\Rightarrow \frac{\partial^3 w}{\partial z \partial t^2} + g \nabla_H^2 w + F^2 \frac{\partial w}{\partial z} = 0$$

which is the vertical velocity equation at the free surface.

C. The Horizontal Structure of Internal Waves

This short theoretical review would be incomplete without a quick description of the horizontal structure of internal waves in the equatorial region.

Using the method of separation of variables on equations (1) through (4) (for example, let $u = \sum_k u_k w_k(z)$ and $v = \sum_k v_k w_k(z)$ where w_k is the vertical structure), one obtains a new system of equations which allows free wave solutions. There are several types of free waves possible which are represented in the dispersion diagram (figure 1).

The Kelvin wave is the simplest solution. Its meridional velocity is null and its amplitude is maximum at the equator, decreasing exponentially towards the turning latitudes. The Kelvin wave, trapped at the equator, propagates eastward without dispersion. Its dispersion relation is: $w = kc$

In addition to the Kelvin waves, there is an infinite number of equatorially trapped waves. These waves are linear combinations of Hermite polynomials H_n. These functions oscillate about the equator and are exponentially decreasing away from it. One type of waves is the inertia-gravity waves which have the following dispersion relationship: $\omega^2 - k^2 = 2n+1$

They are dispersive and may propagate westward or eastward. The dispersion relation for Rossby waves is: $k^2 + k/\omega + 2n+1 = 0$

The short Rossby waves are dispersive and propagate eastward. They are relatively slow. The faster long Rossby waves propagate westward. One last category is the Rossby-gravity wave (or Yanai wave) whose dispersion relation is: $k^2 + k/\omega - \omega^2 +1 = 0$

This wave behaves as a short Rossby wave at low frequencies and as a gravity wave at high frequencies.

Mathematically, these horizontal structures are associated with vertical structures to form the particle velocities u, v and w.

III REGION AND MEANS OF STUDY

The area of study is the tropical Pacific ocean; more precisely, the region between 30°N and 30°S and between 120°E and 90°W. The equatorial region acts as a waveguide since the Coriolis parameter vanishes at the equator and is, therefore, an important area of study.

The first five vertical baroclinic modes are calculated for the entire region of study every degree of latitude and longitude. The bottom depths are obtained from a bathymetry file. Density profiles are provided by a file constructed from the Levitus (1982) Climatological Atlas of the World Ocean. A one degree latitude-longitude grid was used.

Another temperature-salinity file, besides the Levitus file, was necessary for more precise local examinations, since its vertical resolution is rather coarse, especially at depth (e.g. 8 data points available in the 2000m-5500m depth interval). Hence, the NODC Compressed CTD/STD Data file provided the extra data needed. From this file, three regions are sorted out. Each is a 4° by 4° area centered about the following positions: 8°N-150°W, 12°N-138°W and 15°N-125°W. The first file consists of 33 profiles; the second file consists of 33 profiles and the last one consists of 9 profiles. On a mean there are 80 depth levels in each file.

The program used to calculate the vertical modes was written by Julian P. McCreary and modified by Joel Picaut with the help of François Masia. Basically, the mode functions are iterated until convergence is obtained. A minimum depth of 500 m and a maximum of 7000 m were set. The ORSTOM Center Sun computer system was used to perform all the necessary calculation.

IV GENERAL DESCRIPTION OF THE FIRST FIVE VERTICAL MODES IN THE TROPICAL PACIFIC

Figures 2 to 11 are contour plots of phase speeds and surface amplitudes (as defined by Cane, 1984) of modes 1 through 5. One immediately notices tightly packed contour lines in the south-west as well as along the continents. Intuitively, one would suggest that the bottom profile is responsible for such steep gradients. Indeed, the bottom topography in the south-west Pacific is very uneven. Hence, the modes calculated in that region do not have much physical meaning. One of the assumptions made in order to perform theoretical calculations was that the vertical velocity is null at the bottom. But if a steep bottom slope exists, velocity will not be negligible since there will be a possibility for the existence of vertical currents at the bottom point. Thus, one should be extremely careful when considering the results obtained in the south-west equatorial Pacific.

A trend visible in each graph is an increase in speed from east to west. One would suppose that this zonal increase is due to the fact that waters in the eastern Pacific are in general shallower than waters in the western Pacific. We shall show later on that this increase is in fact mainly explained by the way the density profiles change from east to west.

For mode 1, the velocities range from 180 cm/s to 300 cm/s. For the second mode, they range from 100 cm/s to 150 cm/s. The third mode values are spread out over the interval 70 cm/s - 100 cm/s, the fourth mode values over 54 cm/s - 80 cm/s and the fifth mode values over 40 cm/s - 60 cm/s. The surface amplitudes vary from 2.0 cm to 5.0 cm.

V   INFLUENCE OF BOTTOM DEPTH AND OF DENSITY STRUCTURE ON THE CALCULATION OF VERTICAL MODES

The influences of bottom depth and of density profiles on the calculation of vertical modes have been estimated by using a flat bottom and a mean density profile for the tropical Pacific ocean. The mean bottom depth was calculated for the region of interest (and was found to be 3570 m). The mode calculation program was then run with a flat bottom (the desired depth was reached by extrapolation or by cutoff). Figures 12 through 16 represent the contour plots of the modes (1 through 5) obtained in this manner. Since depth is constant, only density profiles can be held responsible for the contours observed. Again, as one proceeds from east to west, the mode values increase. Hence, the distribution of density profiles in the tropical Pacific is in great part responsible for the trend observed in figures 2 through 6.

This finding is reinforced by the contour plots obtained for the modes calculated with a mean density profile for the area of interest (figures 17 through 21). The effect of bottom topography on the calculations appears to be less significant than the effect of varying intensity profiles. Thus, this general increase in modes from east to west is due to the variation in vertical density structure from east to west.

From these last five figures, one can notice that bottom topography is most influential on the west of the region studied. In this region, the bottom changes depth rapidly even though it is not necessarily the deepest. Thus, it seems that the actual depth plays only a minor role in the calculation of modes.

One may also notice that, at higher latitudes (for the contour plots with flat bottom), that's to say around 10°-15° and 25°-30°, the mode velocities do not vary much zonal.This is due to the fact that density profiles along a given latitude in those regions are similar to each other as seen by inspection of Emery et al. (1984), geographic distribution of Brunt-Vaisala frequency profiles in the north Pacific.

Qualitatively, we know that an increase in bottom depth will cause an increase in phase speed. But, how much will the mode be changed if one varies the bottom depth? Observation of the contour plots with mean Levitus density profile in comparison to contour plots with flat bottom shows that the use of a flat bottom doesn't change the mode values as much as the use of a mean density structure. A better quantitative grasp is possible by calculating the mean change in the modes when one uses the uniform bottom instead of the real depths[1]. For the phase speeds the use of a mean depth causes only a 6% change. On the other hand, the use of a mean density profile causes 28% change. For the amplitudes, the use of a flat bottom yields a mean change of 11% whereas a change of 37% is obtained when using a mean density profile. Clearly, the influence of the bottom depth is relatively small.

Figures 23 through 27 show the contour plots of the differences obtained between real modes and modes calculated with a uniform depth. The comparison of these figures with figure 22 (which is the contour plot of the differences between real depths and mean depth for the area of interest) is interesting in that the differences in modes are in no fashion proportional to the differences between real depths and mean depth. Most of the phase speed differences over the region considered are relatively small (5 to 20 cm/s) except close to the continents and in the south-west Pacific where differences reach 160 cm/s for mode 1. Thus, the bottom has a non negligible influence in these regions. It

---

1. * Percentages are obtained by dividing the difference in modes by the real mode value.

would not be wise to replace a real depth by an average bottom depth in these particular cases, since it could result to up to 50% error. But, as pointed out in section IV, one should be extremely careful when calculating modes in this region.

Contour plots were also made for the differences between real modes and modes calculated with a mean Levitus density profile. The south - west part of the region of interest does not stand out as much as in the previous graphs. And, in general, the differences are larger. The calculation of a mean ratio shows that differences between real modes and "mean density modes" are about 5 times larger than the differences caused by the use of a mean depth.

Further investigation into the problem of quantifying the influences of bottom depth and density on mode calculations was performed by correlating the modes obtained with a mean depth and the real modes (figures 28 through 32). Correlations were also made for the modes calculated with a mean density profile (figures 33 through 37). For all the correlations, the area of study was reduced to 170°E - 110°E in order to eliminate all the erroneous data points provided by the south - west region.

The slopes of the linear regression lines reveal once again that density plays a greater role than bottom depth. If the correlation coefficients were all as good as the one for figure 28, information on the extent to which the bottom depth and density influence mode calculations would be available.

VI INFLUENCE OF DEEP DENSITY STRUCTURE ON THE CALCULATION OF VERTICAL MODES

Part of the last section dealt with the influence of density structure on the mode calculations. The conclusion that density is, by far, more important than bottom depth was reached. In this section, we examine the influence of deep vertical density structure.

In order to do this, a mean density profile, as well as a mean Vaisala frequency profile, for the entire region of study is obtained. At a given position, the corresponding Vaisala frequency profile is connected at 500 m to the mean profile by linear interpolation over an interval of 200 m. Thus, the actual profile is conserved for the first five hundred meters whereas below 500 m, the profile is the mean Vaisala frequency profile. A vertical mode decomposition is then performed for this connected profile and plotted in order to visualize the vertical modal structure. The vertical modal structure of the actual profile (corresponding to the given position) is also plotted and allows comparison to take place.

Several examples are given in figures 38, 39 and 40. They all show the actual Vaisala frequency profile, the connected profile and the corresponding calculated mode. The errors in using the connected profiles are in the order of 2% to 4% for the phase speeds and surface amplitudes. These errors are estimated as the difference between the values obtained with real and connected profiles, divided by the real profile value. It is interesting to see that the use of the connected profile has very little effect on the modal structure, even at depth. The mode graphs can be superposed nearly perfectly. Hence, the most important information necessary to calculate vertical modes at a given position is the density profile for the first 500 m.

In order to verify these results, the procedure was repeated for the more depth-precise files (see section III) sorted out for the 4° by 4° regions centered around 8°N-150°W. The records contained in this file have very precise depth data which will allow a better examination of the effects of our procedure at depth. Figures 41 through 43 show examples of the results obtained. The phase speeds and surface amplitudes do

not differ more than by 3 to 4%. And even though the vertical modal structures are not as smooth as the ones obtained with the Levitus file, they superpose each other relatively well for a given position.

VII CONCLUSION

There are two important conclusions to be made from the study. First of all, the influence of bottom depth in the modal calculation is negligible as compared to the influence of the density structure. The other major result is that one only needs to possess precise information about the density structure in the top 500 meters in order to calculate accurate modal values (with the help of a mean density profile reaching the bottom for the entire region considered) at a given position.

The statistical reliability of the Levitus file appears to be sufficient (only a few profiles are invalid for modal calculations, mainly due to density inversions). This file provides a handy working tool for the examination of vertical modal structures in the world oceans. Unfortunately, the problem of quantifying the respective influences of density and depth has not been solved satisfactorily.

REFERENCES

Behringer, D. W., 1984: Equatorial Modes in the Eastern Pacific (85°W), *J. Geophys. Res.*, **89**, 3729-3731.

Cane, M. A., 1984: Modeling Sea Level During El Nino. *J. Phys. Oceanogr.*, **14**, 1864-1874.

Emery, W. J., W. G. Lee and L. Magaard, 1984: Geographic and Seasonal Distributions of Brunt-Vaisala Frequency and Rossby Radii in the North Pacific and North Atlantic. *J. Phys. Oceanogr.*, **14**, 294-317.

Gill, A., 1982: Atmosphere - Ocean Dynamics, *Int. Geophys. Ser.*, **30**, Academic Press, 662 pp.

Hayes, S. P., P. Ripa and L. J. Mangum, 1985: On Resolving Vertical Modes with Observational Data, *J. Geophys Res.*, **90**, 7227-7234.

Levitus, S., 1982: Climatological atlas of the world ocean. NOAA Prof. Pap., 13, 173pp., U.S. Government Printing Office, Washington D.C.

Mangum, L., and S. Hayes, 1984: The Vertical Structure of the Zonal Pressure Gradient in the Eastern Equatorial Pacific, *J. Geophys. Res.* **89**, 10441-10449

McCreary, J.P., 1985: Modeling Equatorial Ocean Circulation, *Ann. Rev. Fluid Mech.*, **17**,359-409.

McPhaden, M.J., J.A. Proehl and L.M. Rothstein, 1987: On the Structure of Low Frequency Equatorial Waves. *J. Phys. Oceanogr.*, **17**, 1555-1559.

Pedlosky, J., 1979: Geophysical Fluid Dynamics, Springer - Verlag, 624pp.

Roberts, J., 1975: Internal gravity waves in the ocean. Marcel Dakker, Inc., New York.

Tang, T.Y., R.H. Weisberg and D. Halpern, 1988: Vertical Structure of Low Frequency Variability in the Eastern Equatorial Pacific Ocean. *J. Phys. Oceanogr.*, **18** 1009-1019.

Toole, J., 1985: Near equatorial CTD observations at 85° W in October 1982. *J. Geophys. Res.*, **90**, 929-933.

Toole, J., and M. Borges, 1984: Observations of Horizontal Velocity and Vertical Displacements in the Equatorial Pacific Ocean Associated with the Early Stages of the 1982/1983 El Nino. *J. Phys. Oceanogr.*, **14**, 949-959.
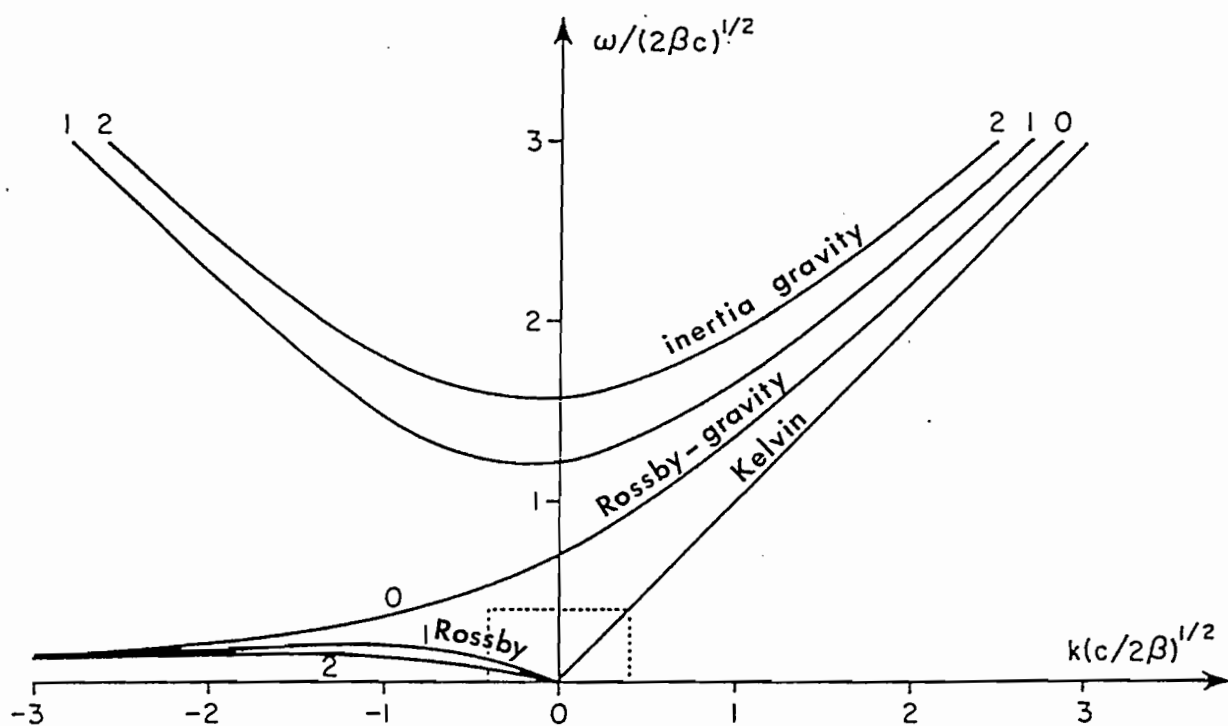
FIG.1.Dispersion diagram (From Gill, 1982).

MODE 1
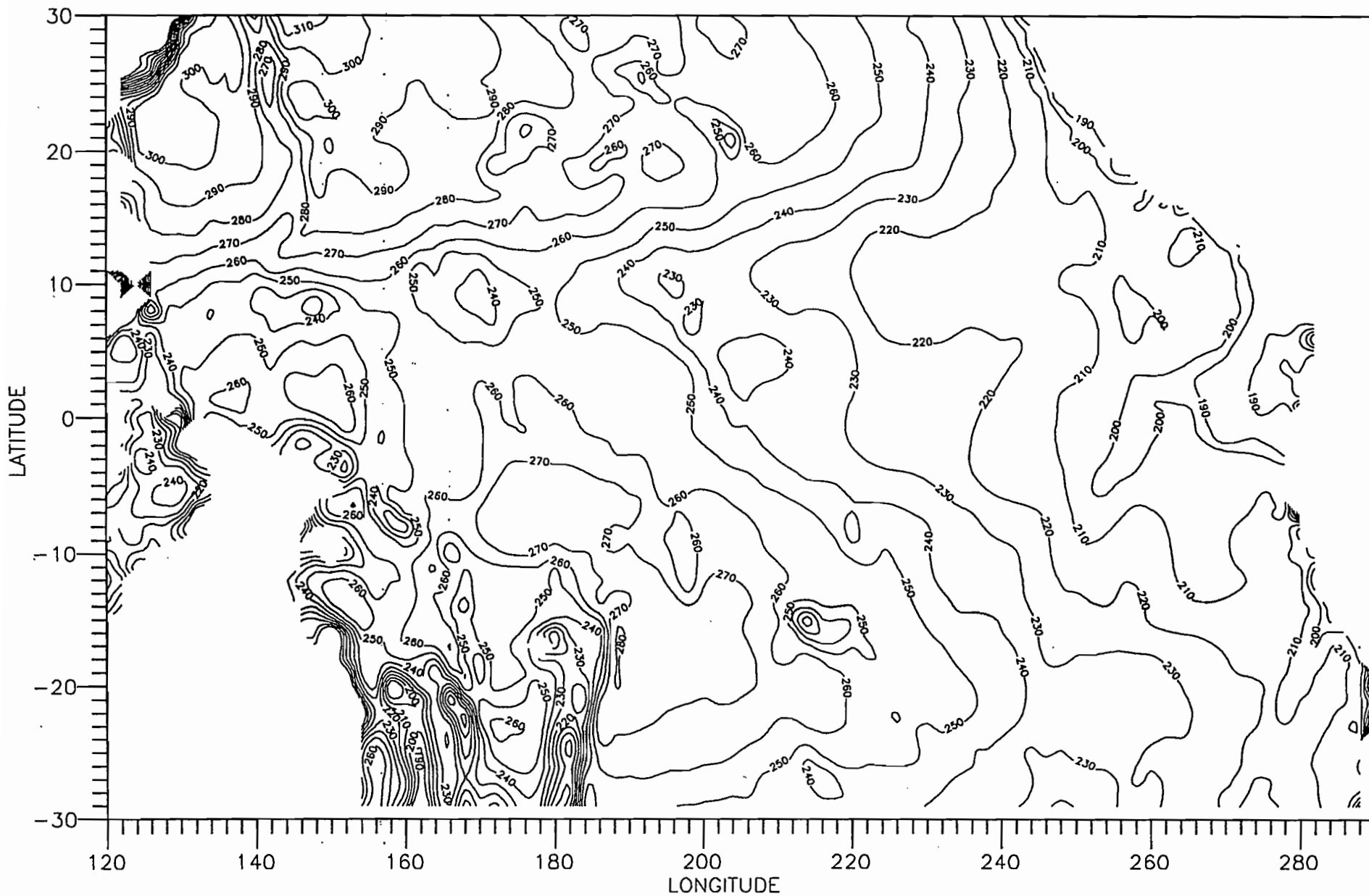
FIG.2.Contour plot of the phase speed (cm/s) for the first baroclinic mode .

MODE 2
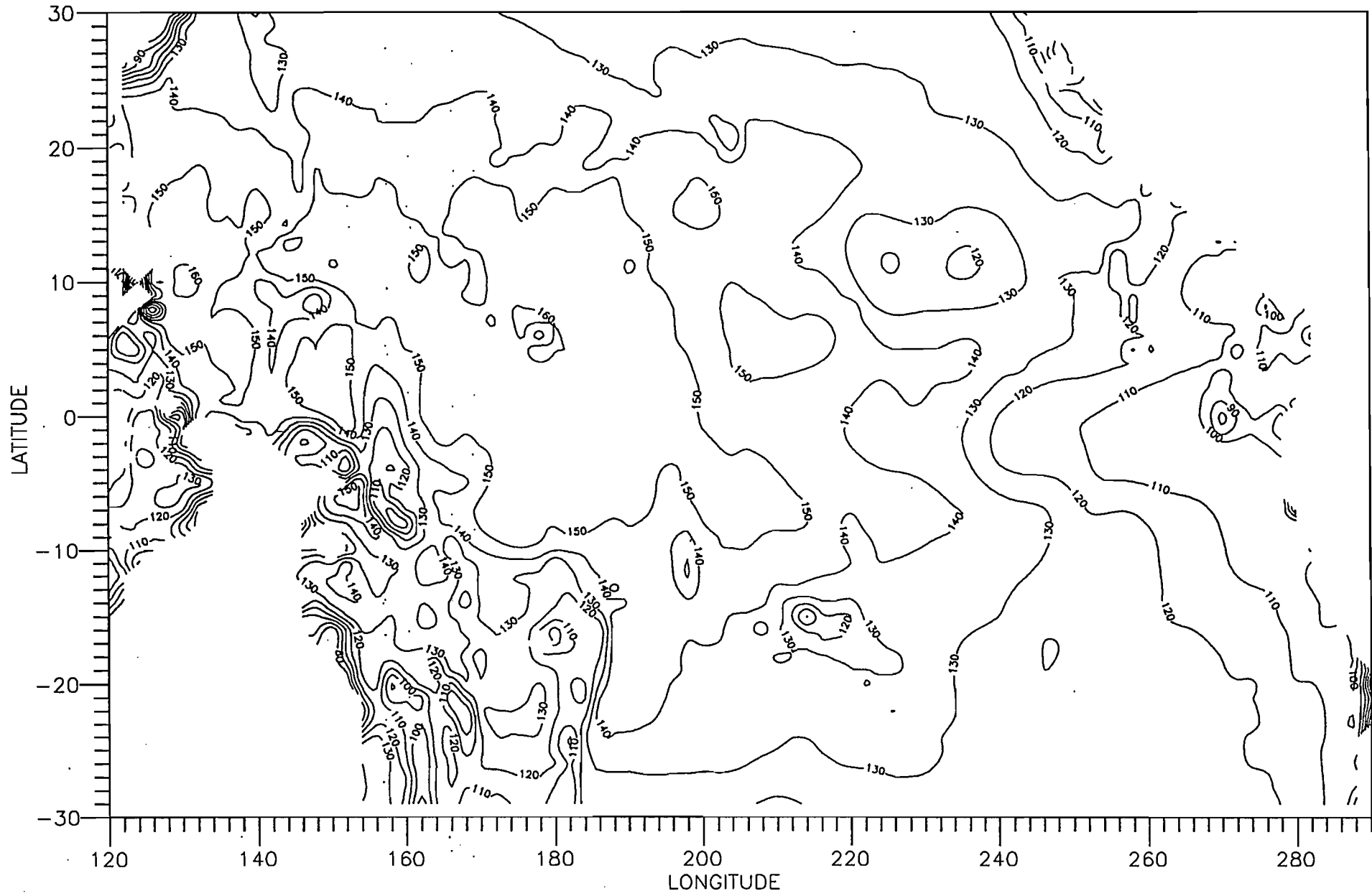
FIG.3.Contour plot of the phase speed (cm/s) for the second baroclinic mode .

MODE 3
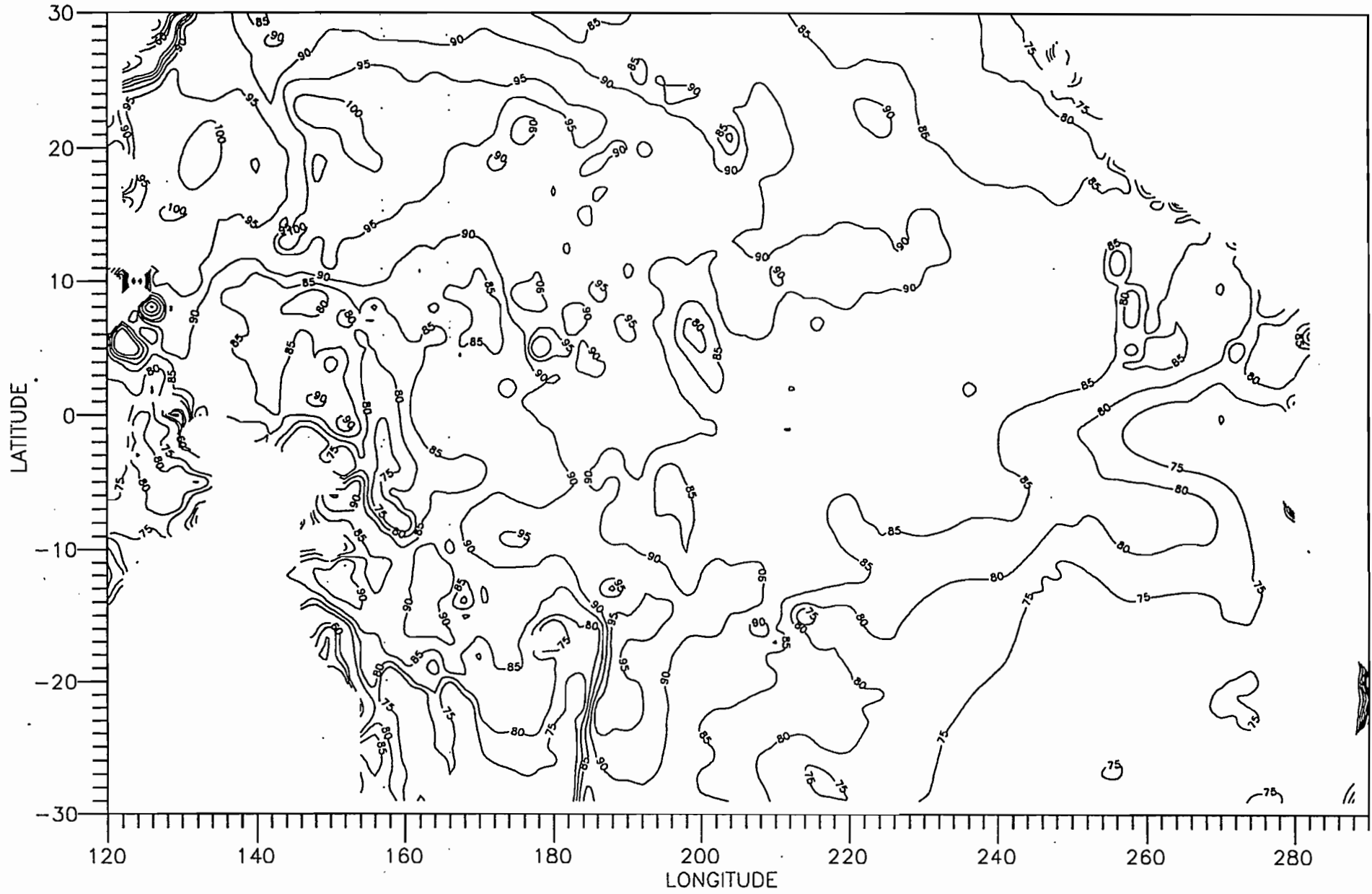
FIG.4.Contour plot of the phase speed (cm/s) for the third baroclinic mode .

MODE 4
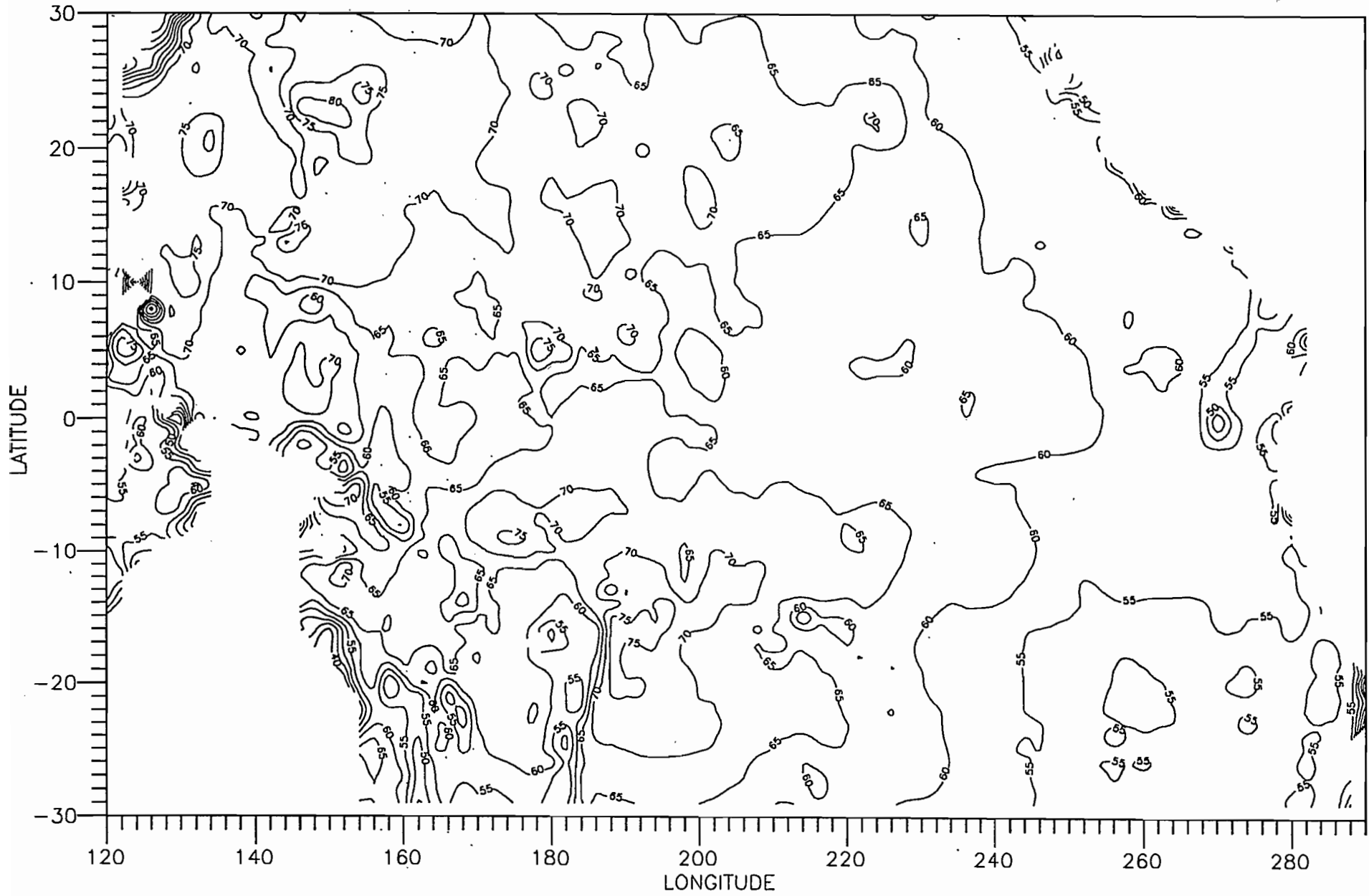
FIG.5.Contour plot of the phase speed (cm/s) for the fourth baroclinic mode .

19

MODE 5
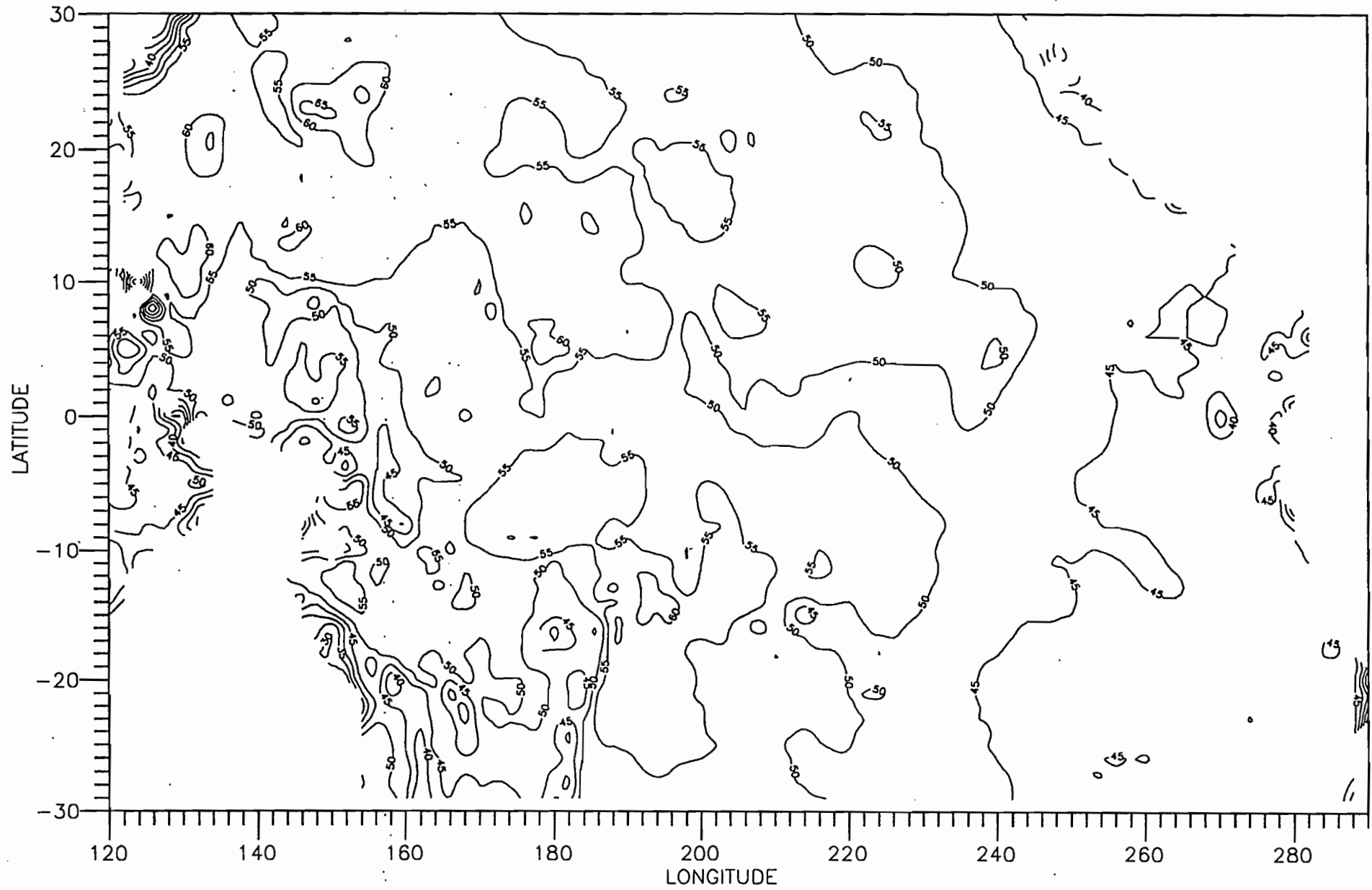
FIG.6.Contour plot of the phase speed (cm/s) for the fifth baroclinic mode .

AMPLITUDE 1
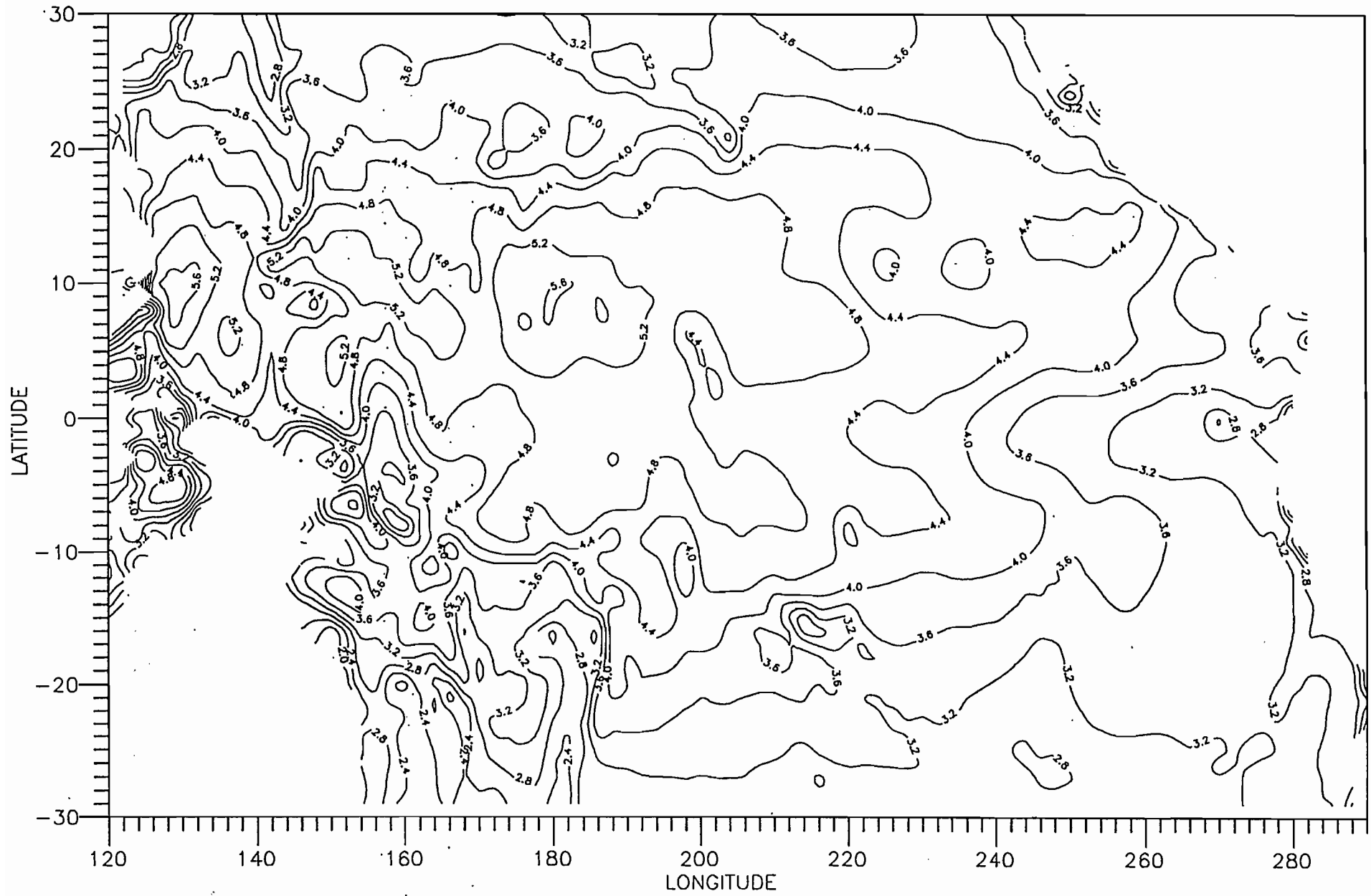
FIG.7.Contour plot of the surface amplitude (cm) for the first baroclinic mode.

AMPLITUDE 2
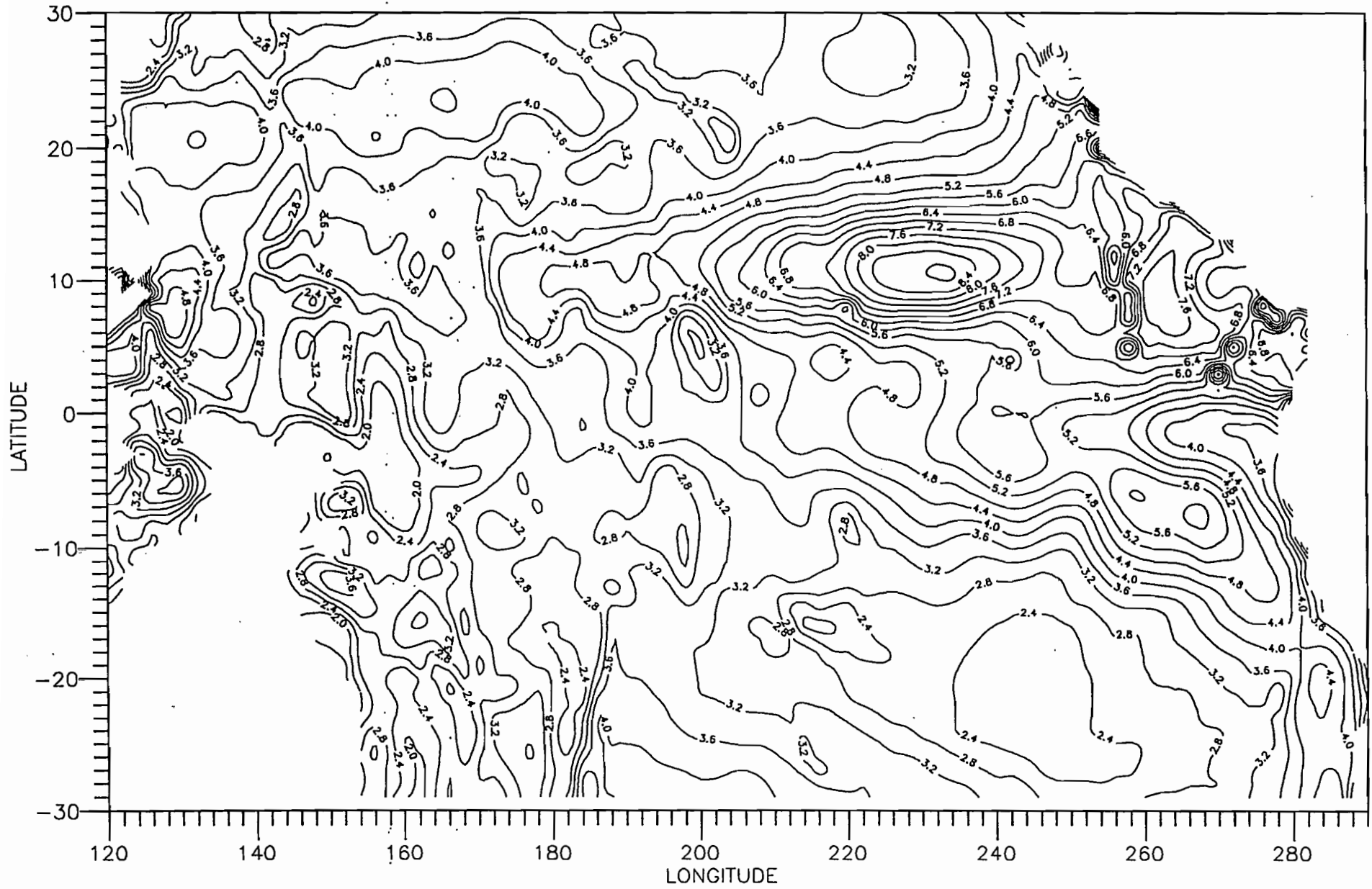
FIG.8. Contour plot of the surface amplitude (cm) for the second baroclinic mode.

AMPLITUDE 3
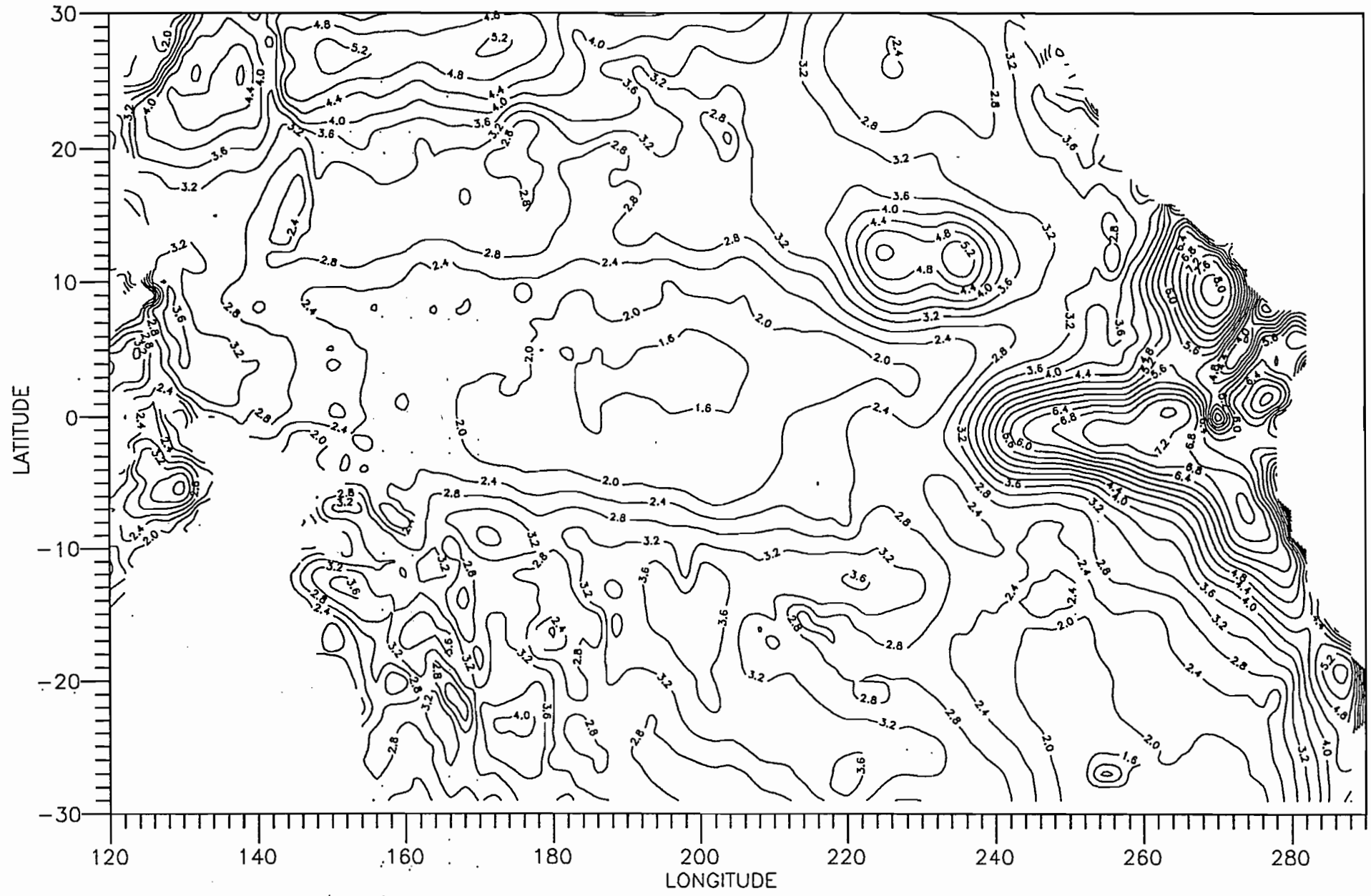
FIG.9.Contour plot of the surface amplitude (cm) for the third baroclinic mode.

23
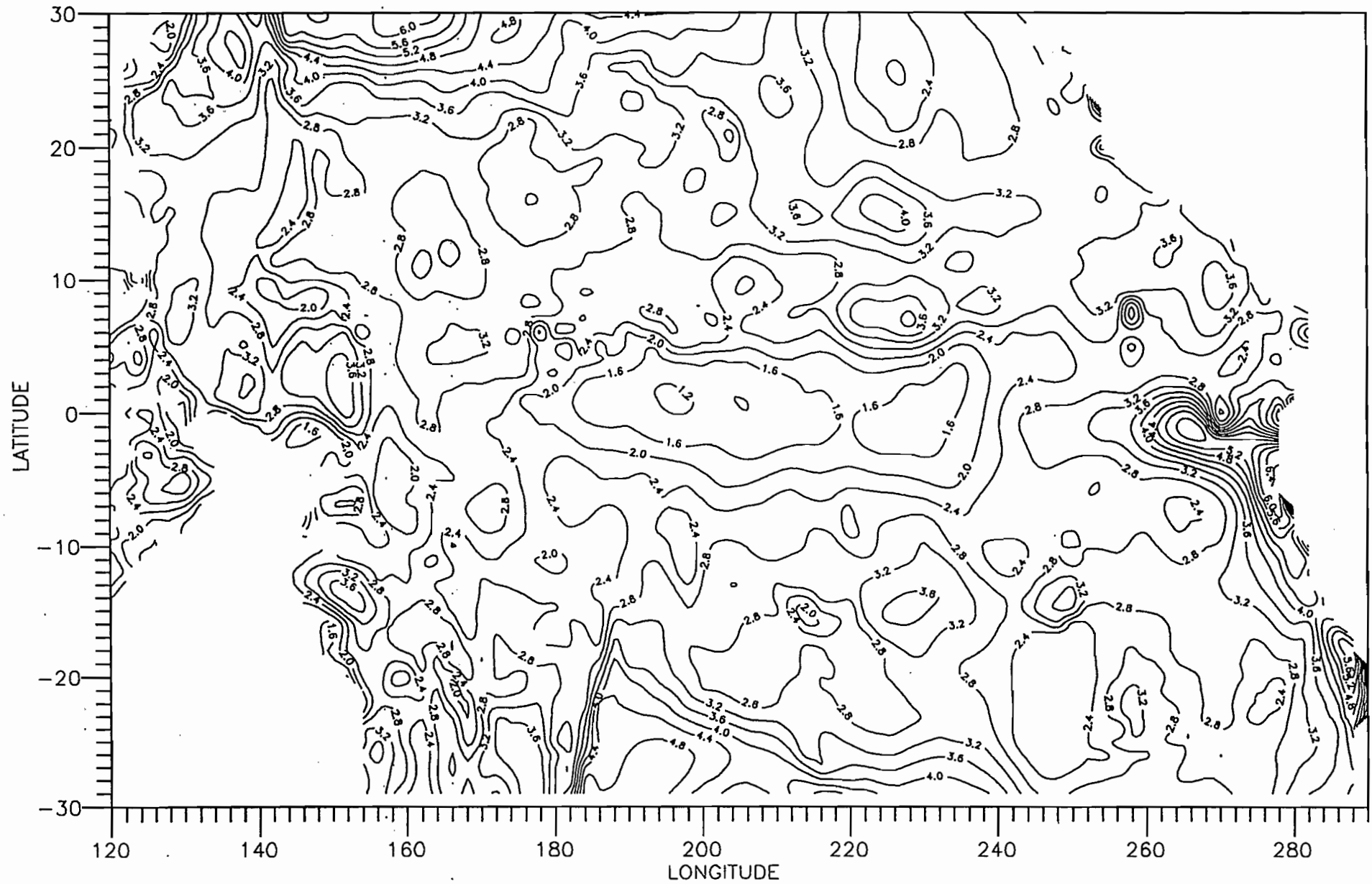
AMPLITUDE 4

FIG.10.Contour plot of the surface amplitude (cm) for the fourth baroclinic mode.

AMPLITUDE 5
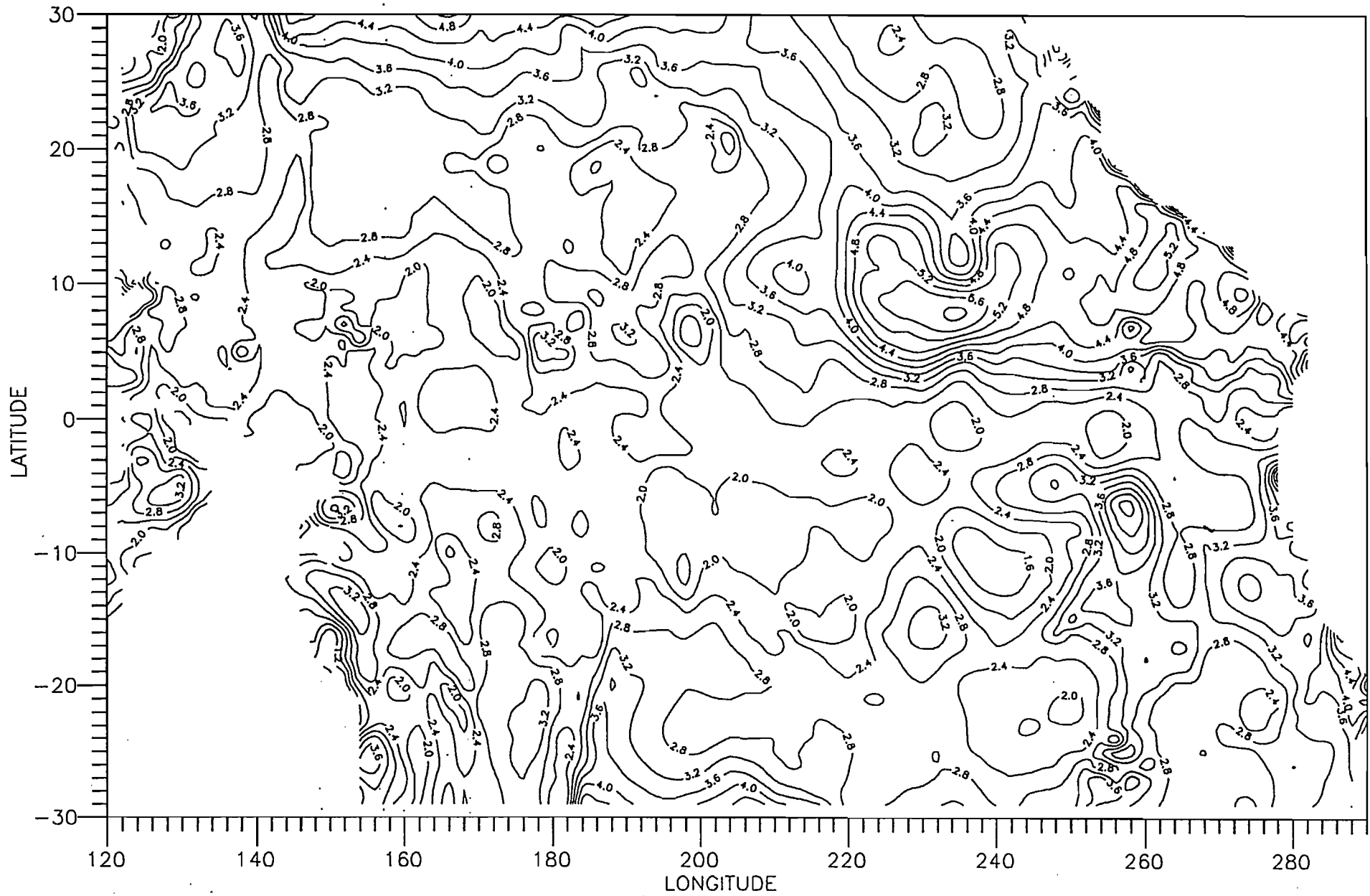
FIG.11.Contour plot of the surface amplitude (cm) for the fifth baroclinic mode.

MODE 1 (Flat bottom = 3570 m)
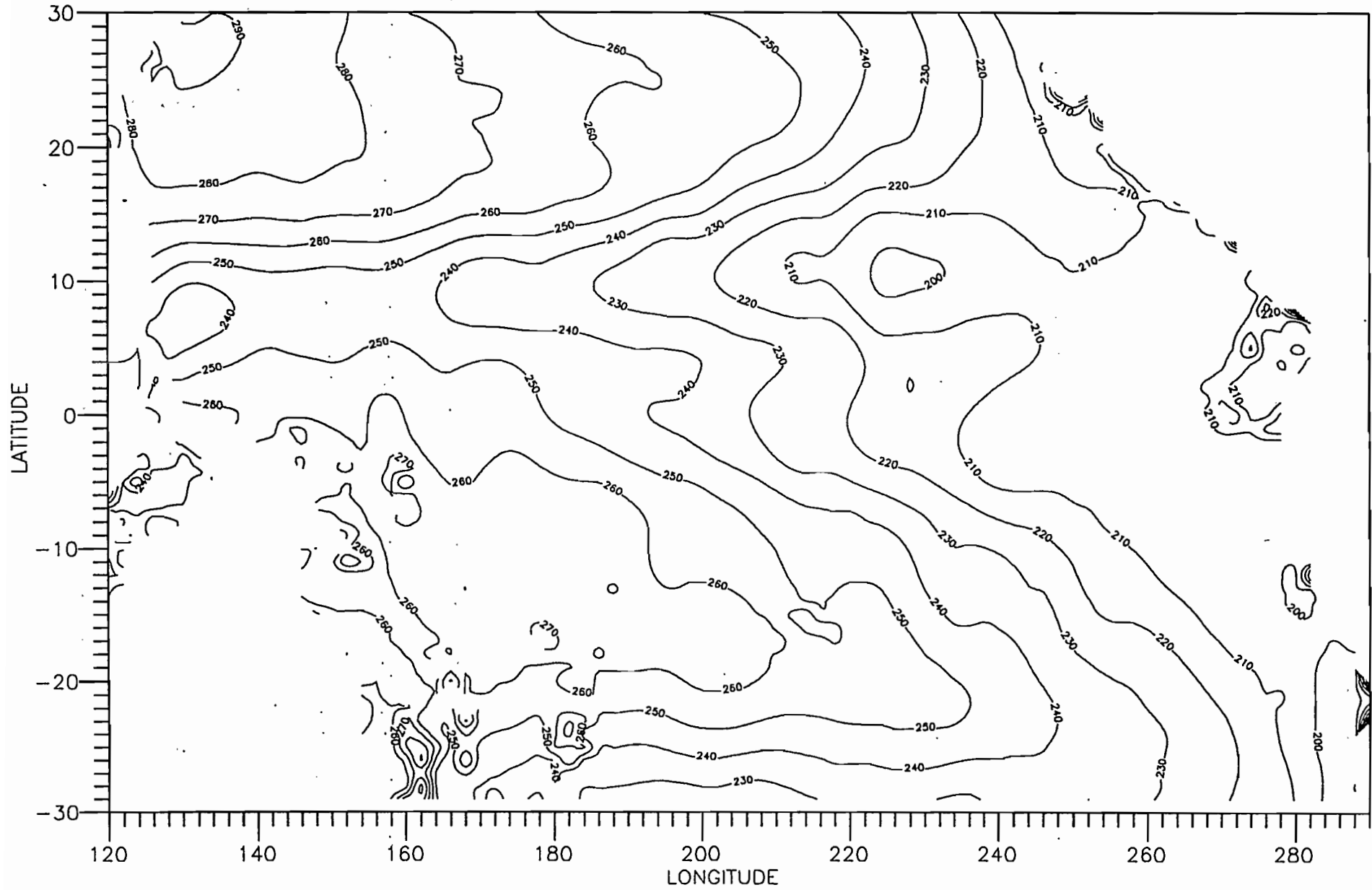
FIG.12.Contour plot of the phase speed (cm/s) calculated with a flat bottom for mode 1.
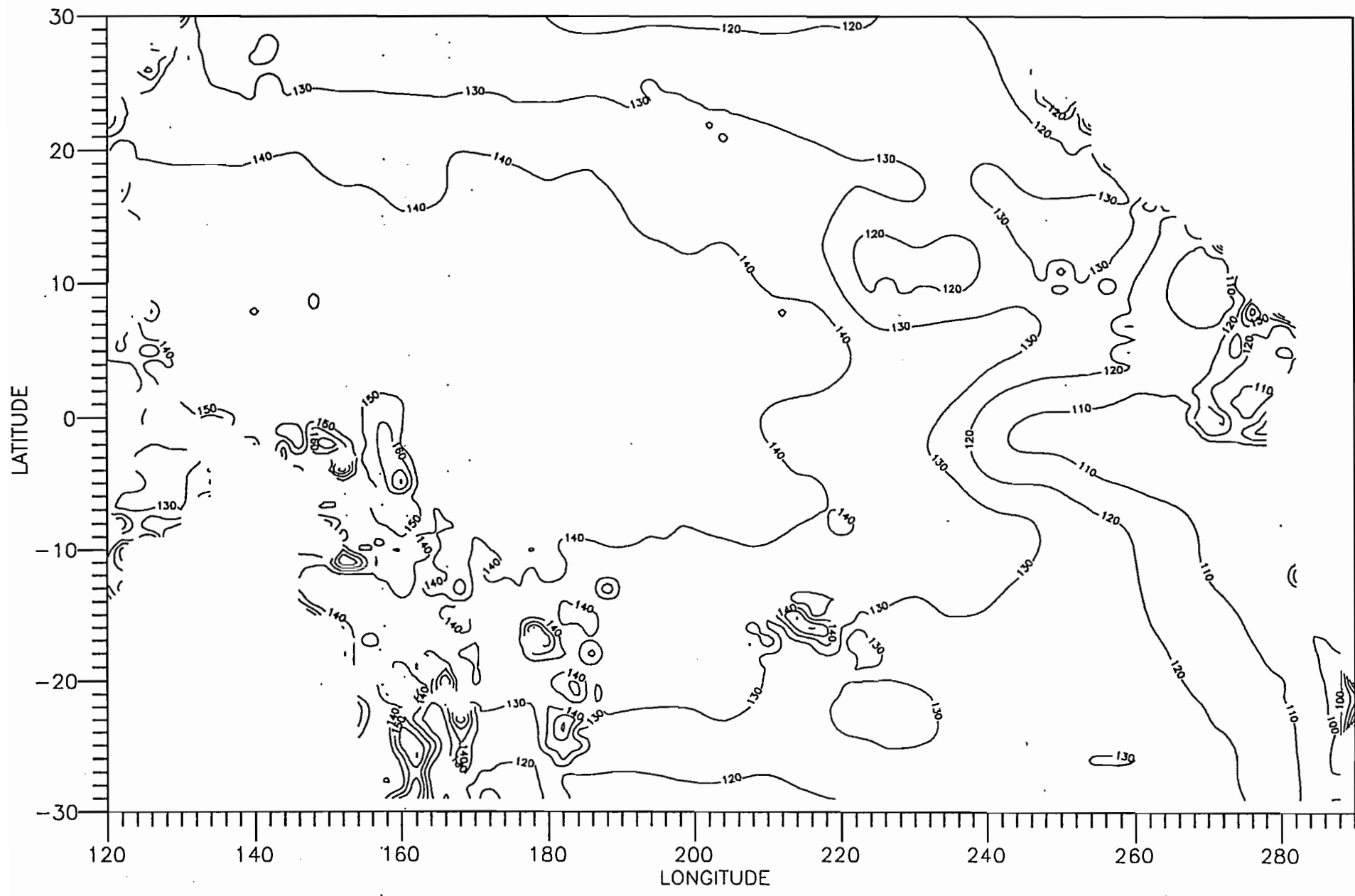
FIG.13.Contour plot of the phase speed (cm/s) calculated with a flat bottom for mode 2.

MODE 3 (Flat bottom = 3570 m)
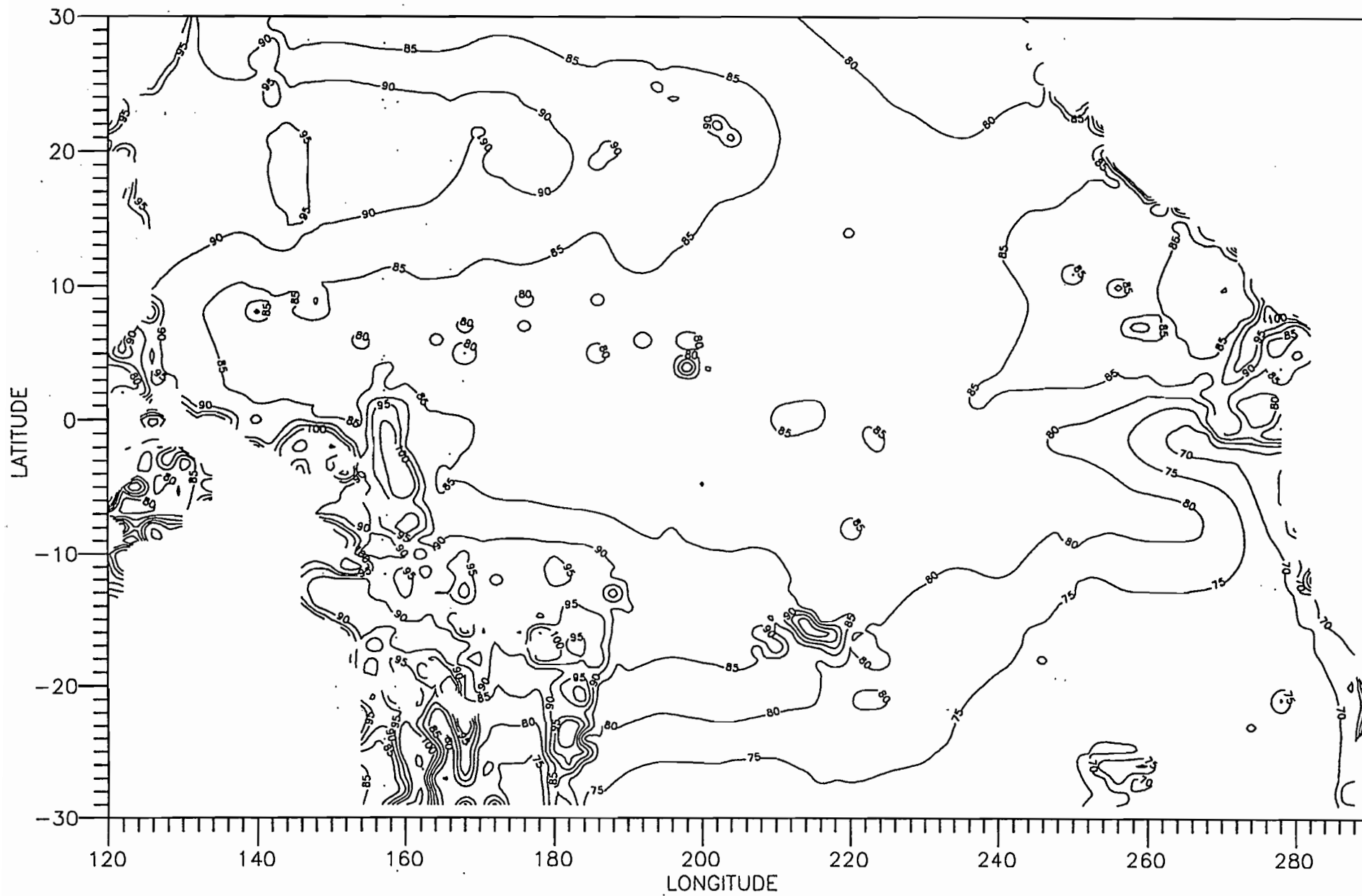
FIG.14.Contour plot of the phase speed (cm/s) calculated with a flat bottom for mode 3.

MODE 4 (Flat bottom = 3570 m)
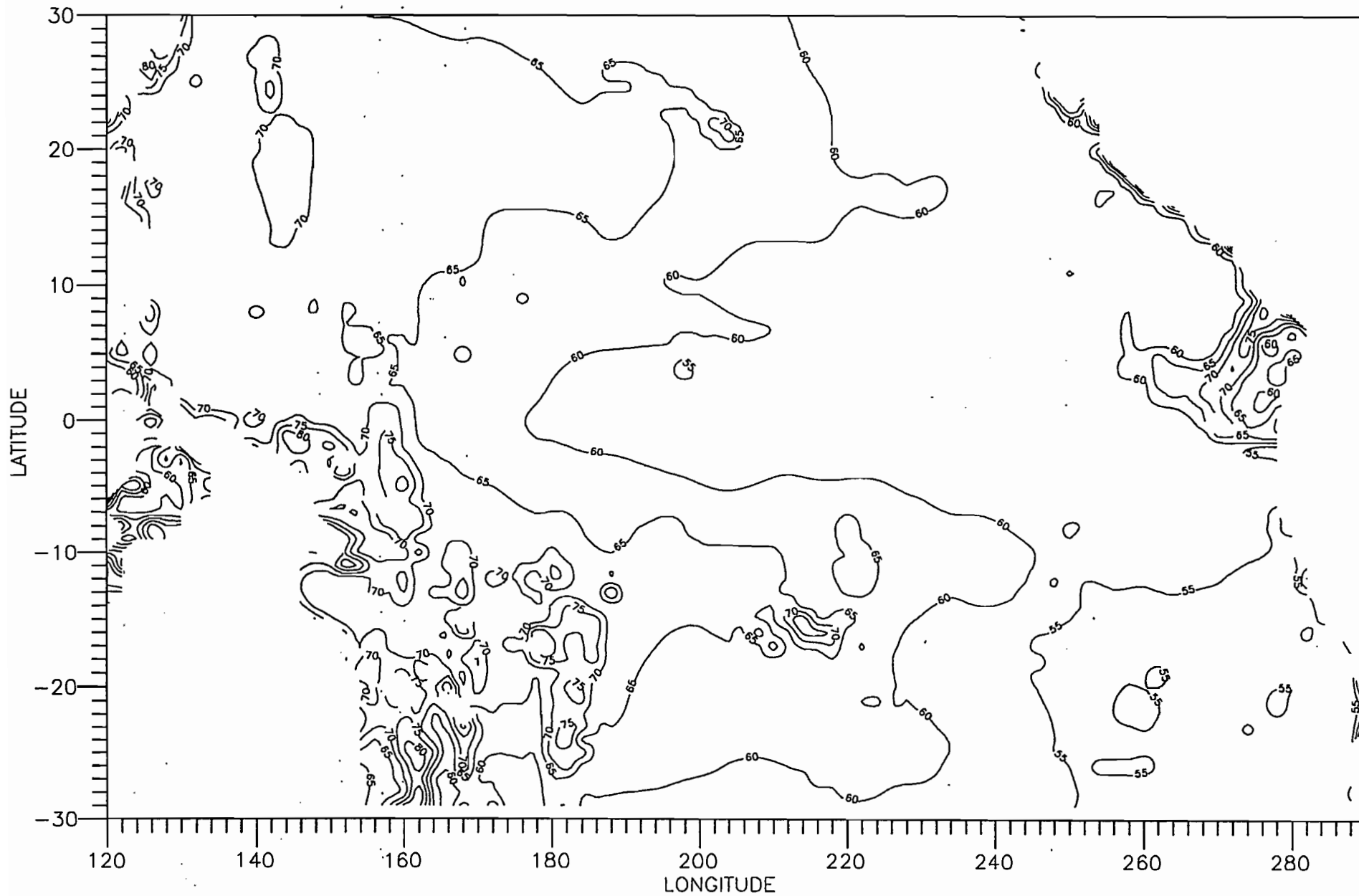
FIG.15.Contour plot of the phase speed (cm/s) calculated with a flat bottom for mode 4.

MODE 5 (Flat bottom = 3570 m)
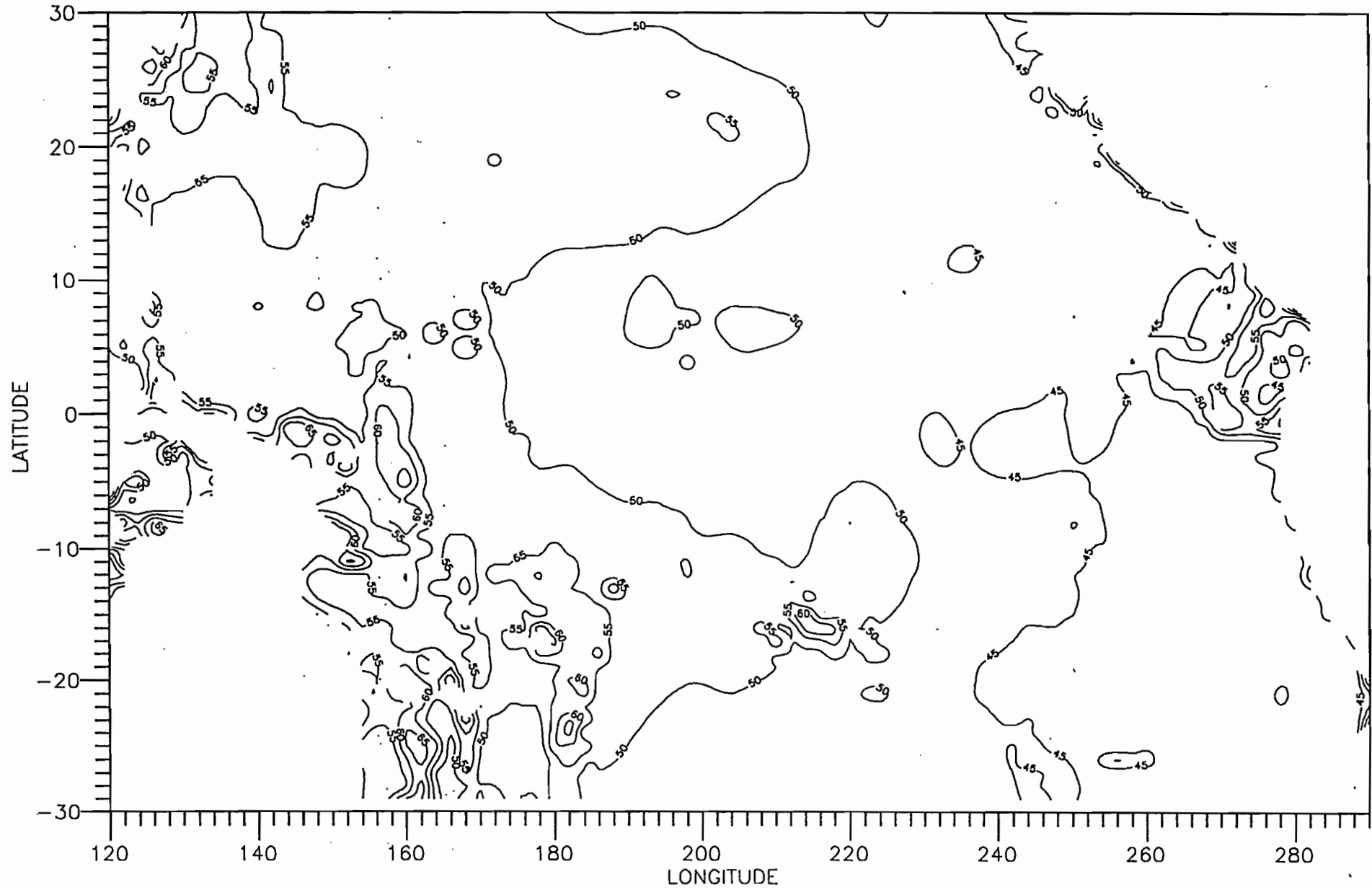
FIG.16.Contour plot of the phase speed (cm/s) calculated with a flat bottom for mode 5.

MODE 1 (Mean Levitus profile)
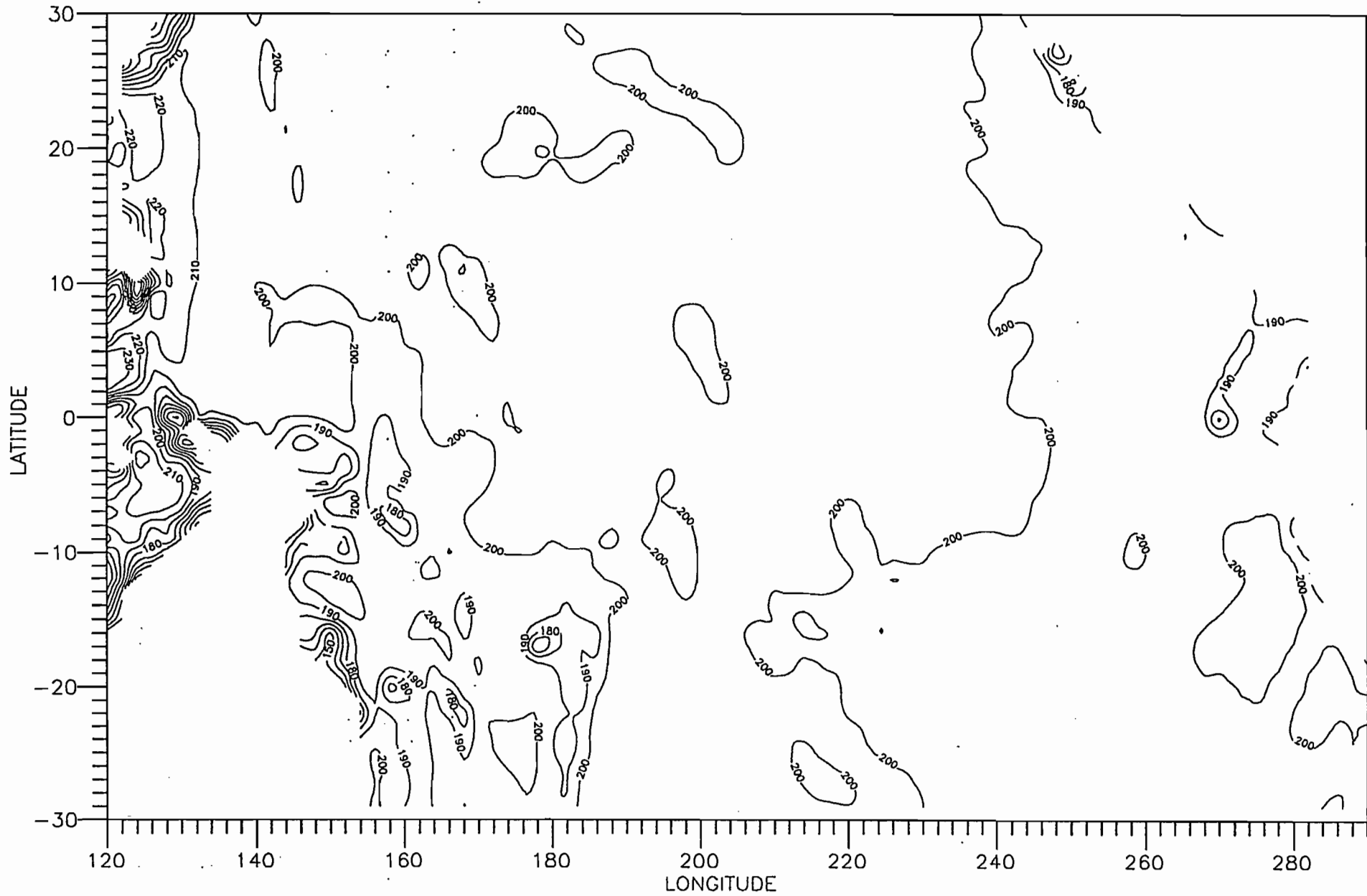
FIG.17. Contour plot of the phase speed (cm/s) calculated with a mean density profile for mode 1.

MODE 2 (Mean Levitus profile)
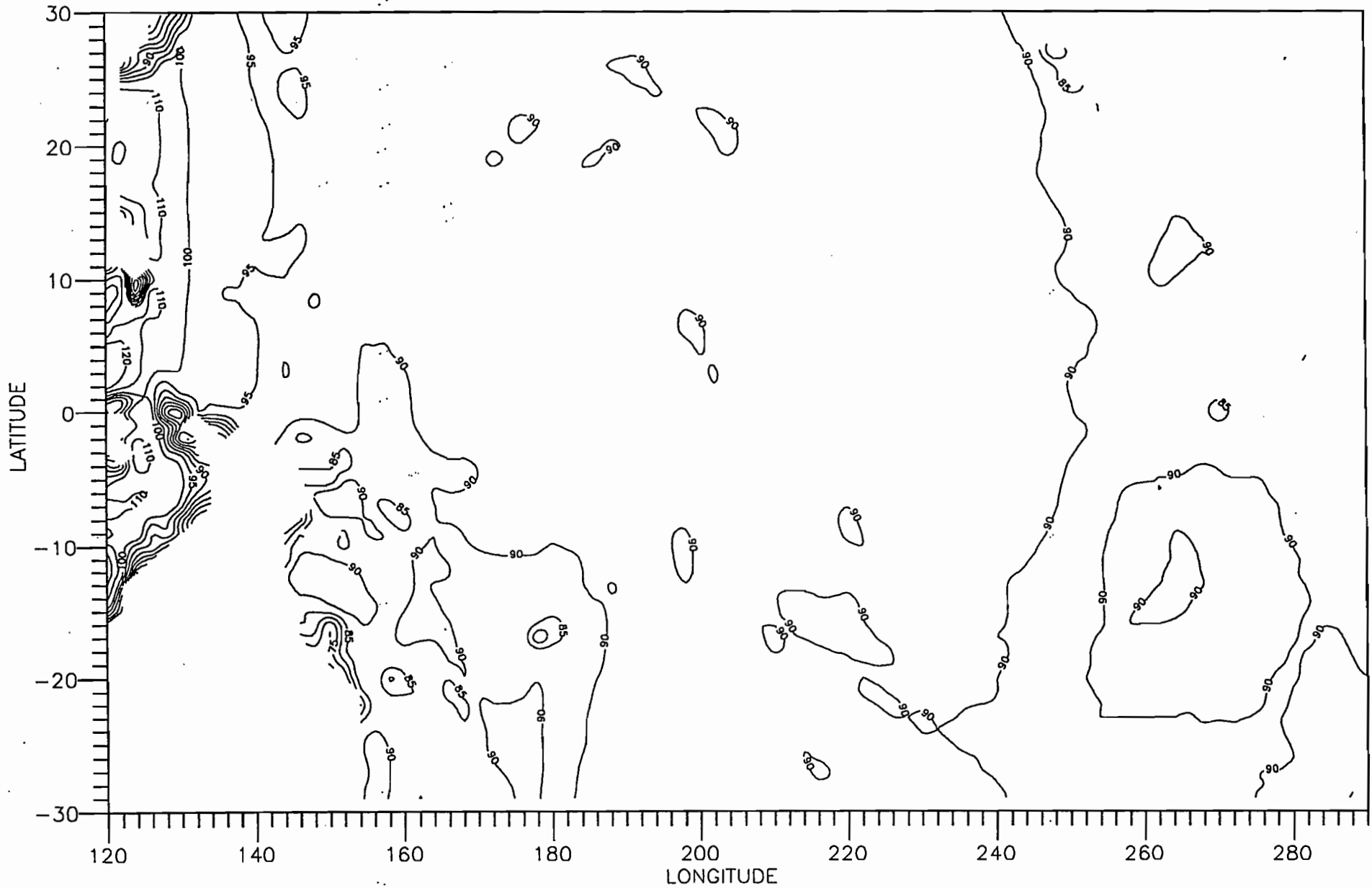
FIG.18.Contour plot of the phase speed (cm/s) calculated with a mean density profile for mode 2.

MODE 3 (Mean Levitus profile)
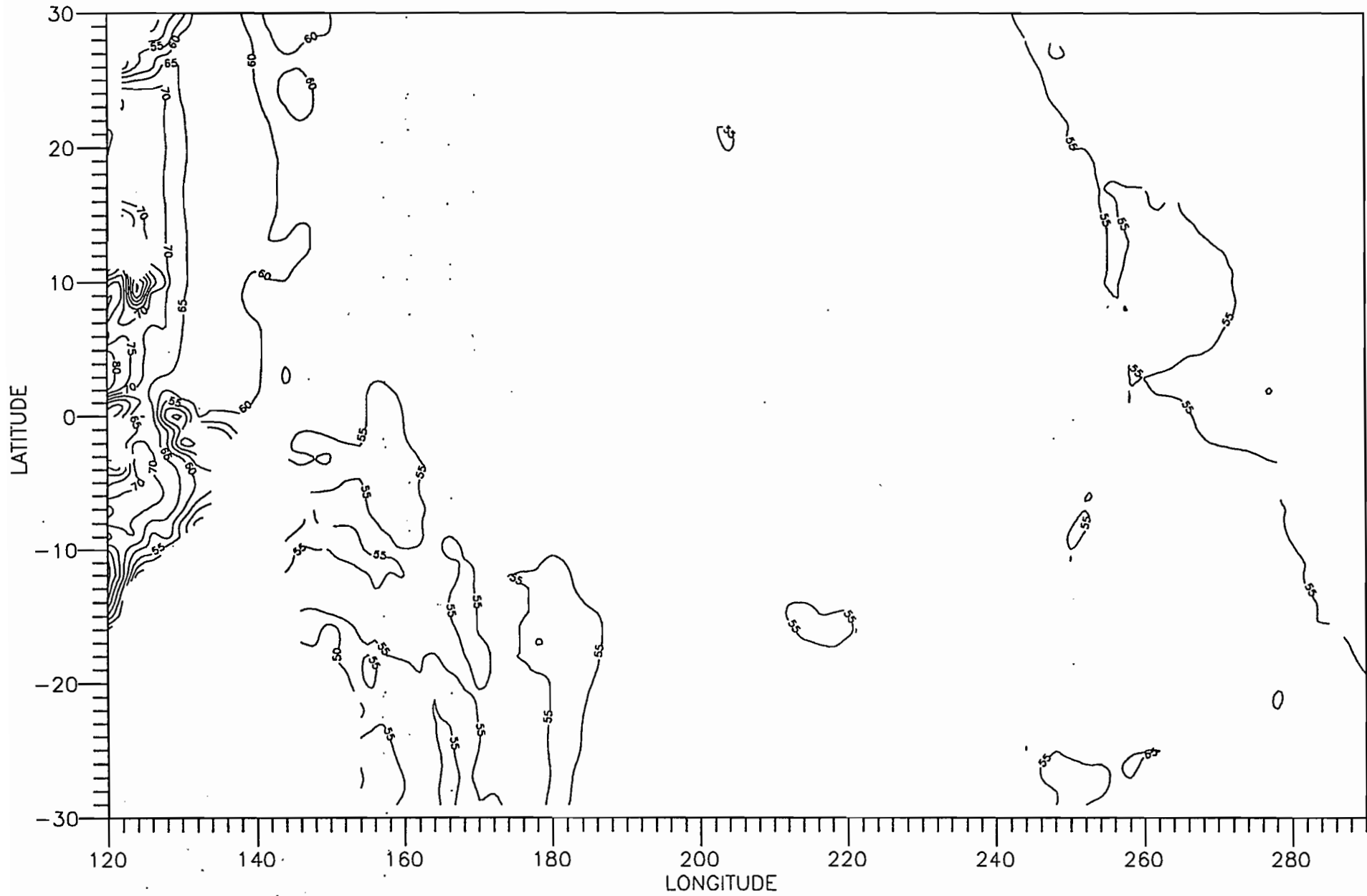
FIG.19.Contour plot of the phase speed (cm/s) calculated with a mean density profile for mode 3.

MODE 4 (Mean Levitus profile)
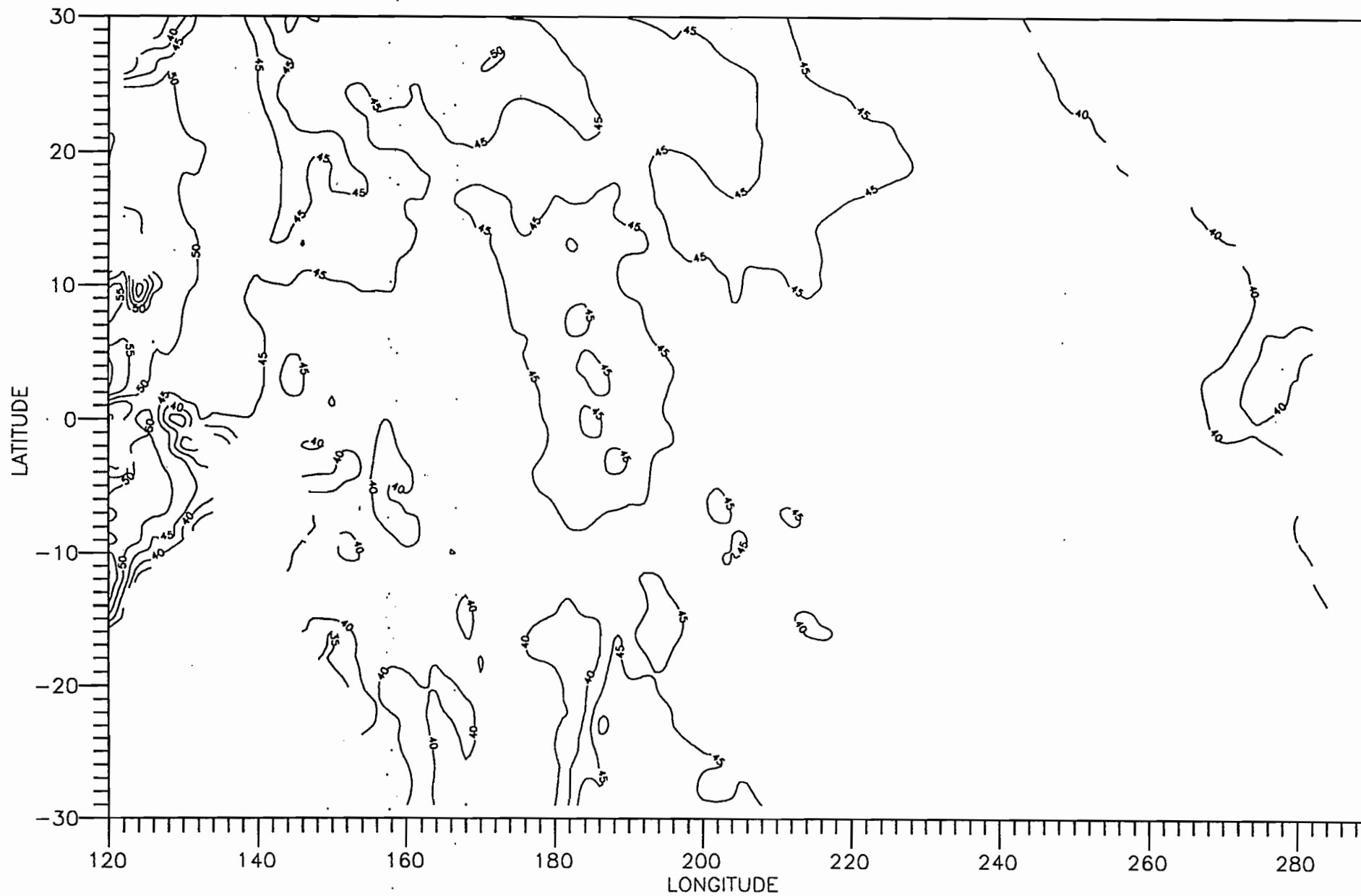
FIG.20.Contour plot of the phase speed (cm/s) calculated with a mean density profile for mode 4.

34

MODE 5 (Mean Levitus profile)

35
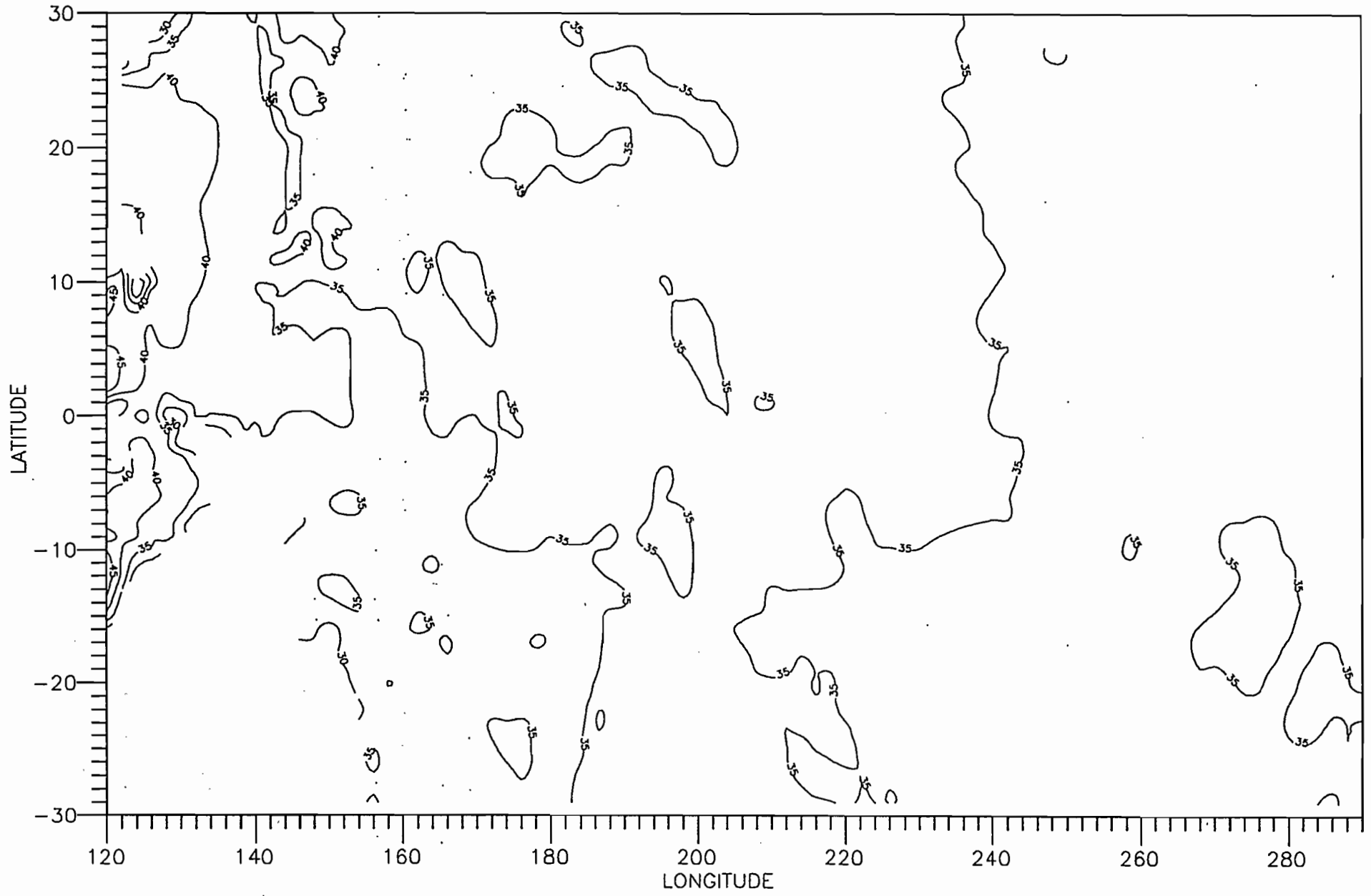
FIG.21.Contour plot of the phase speed (cm/s) calculated with a mean density profile for mode 5.

DIFFERENCES BETWEEN REAL AND MEAN DEPTHS
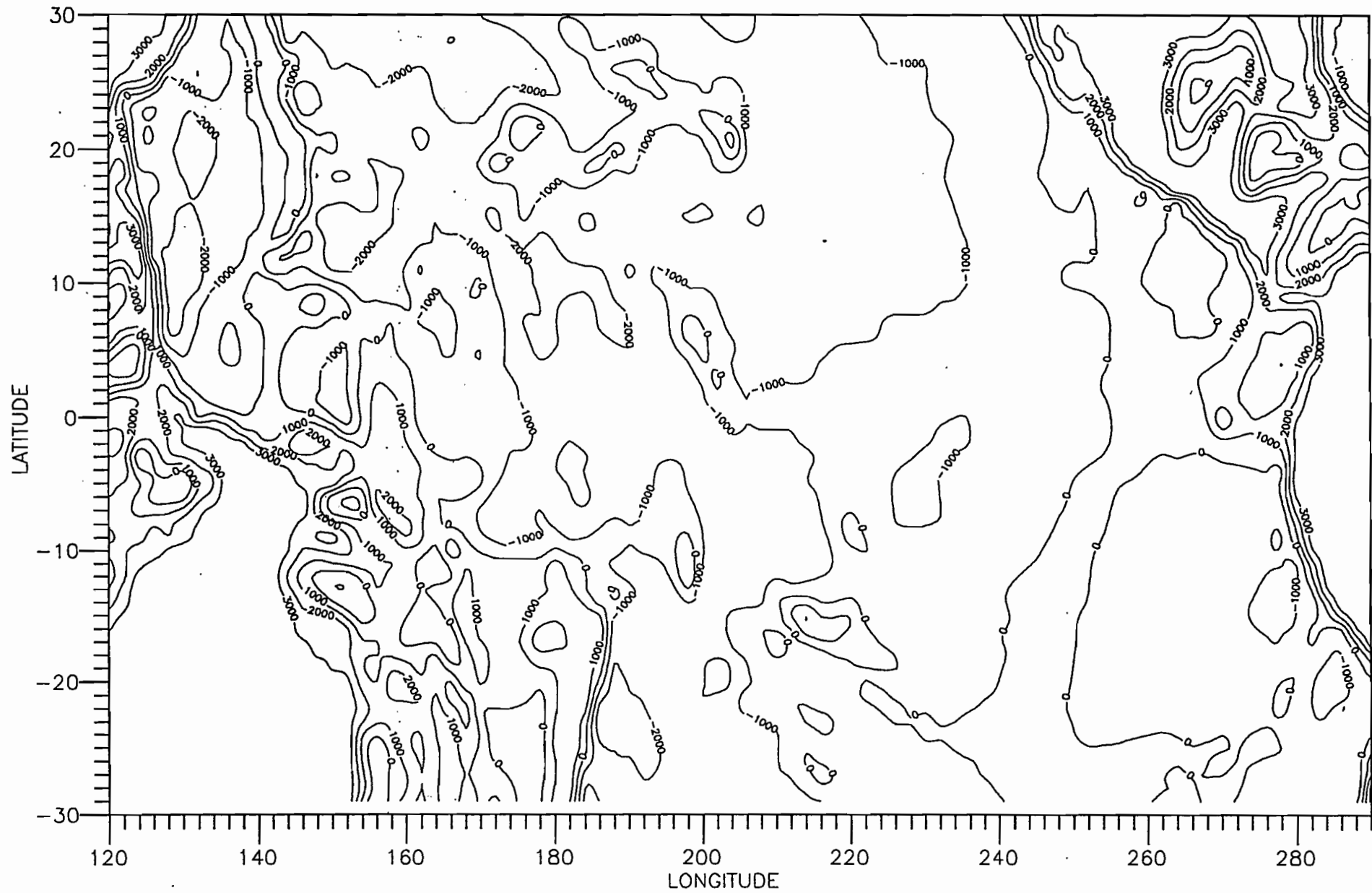
FIG.22. Contour plot of the differences between real and mean depths (in m).

MODE 1 DIFFERENCES (between real and flat bottom)
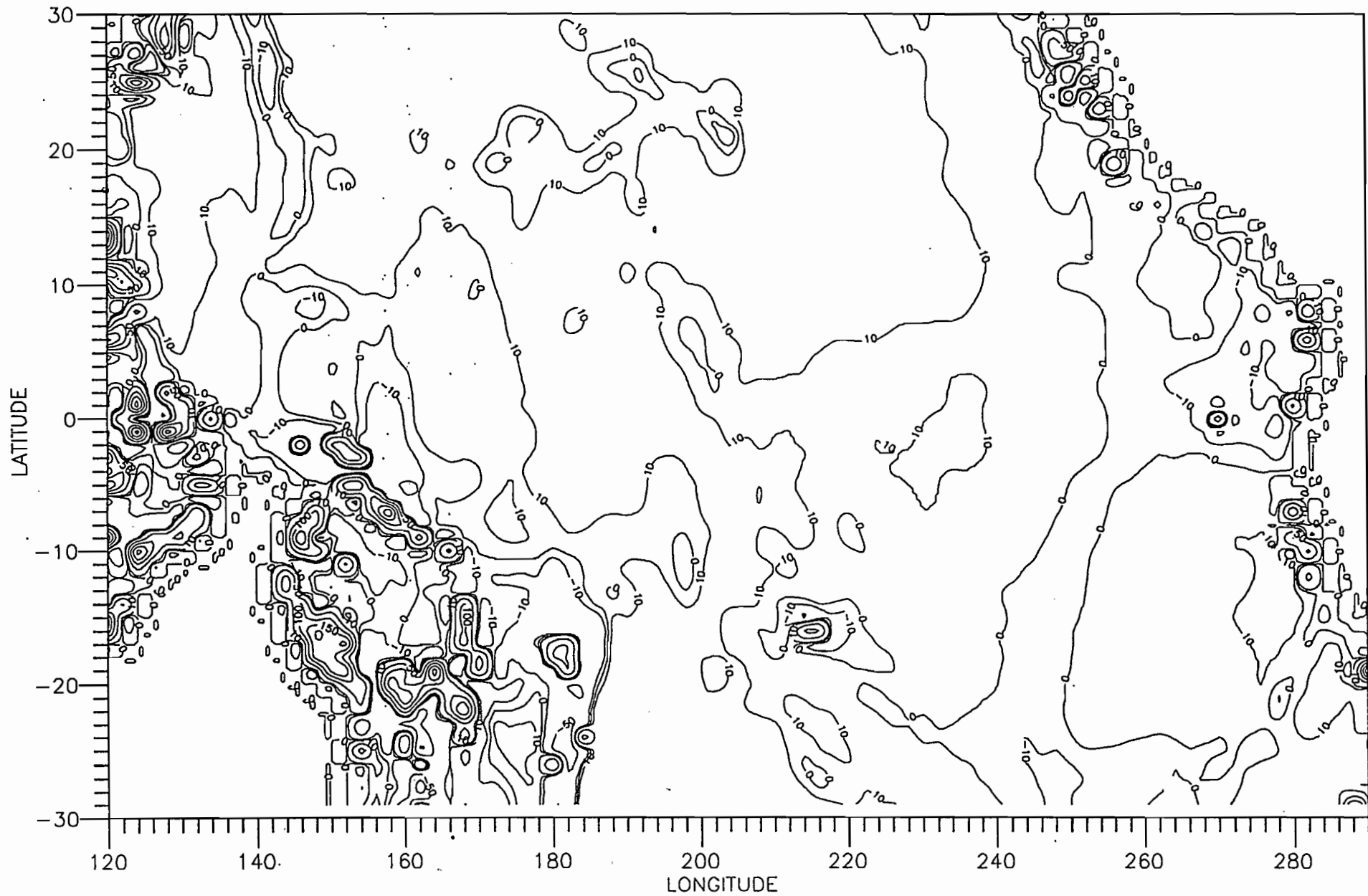
FIG.23.Contour plot of the differences in phase speed (cm/s) for mode 1 when real and mean depths are used.

MODE 2 DIFFERENCES (between real and flat bottom)
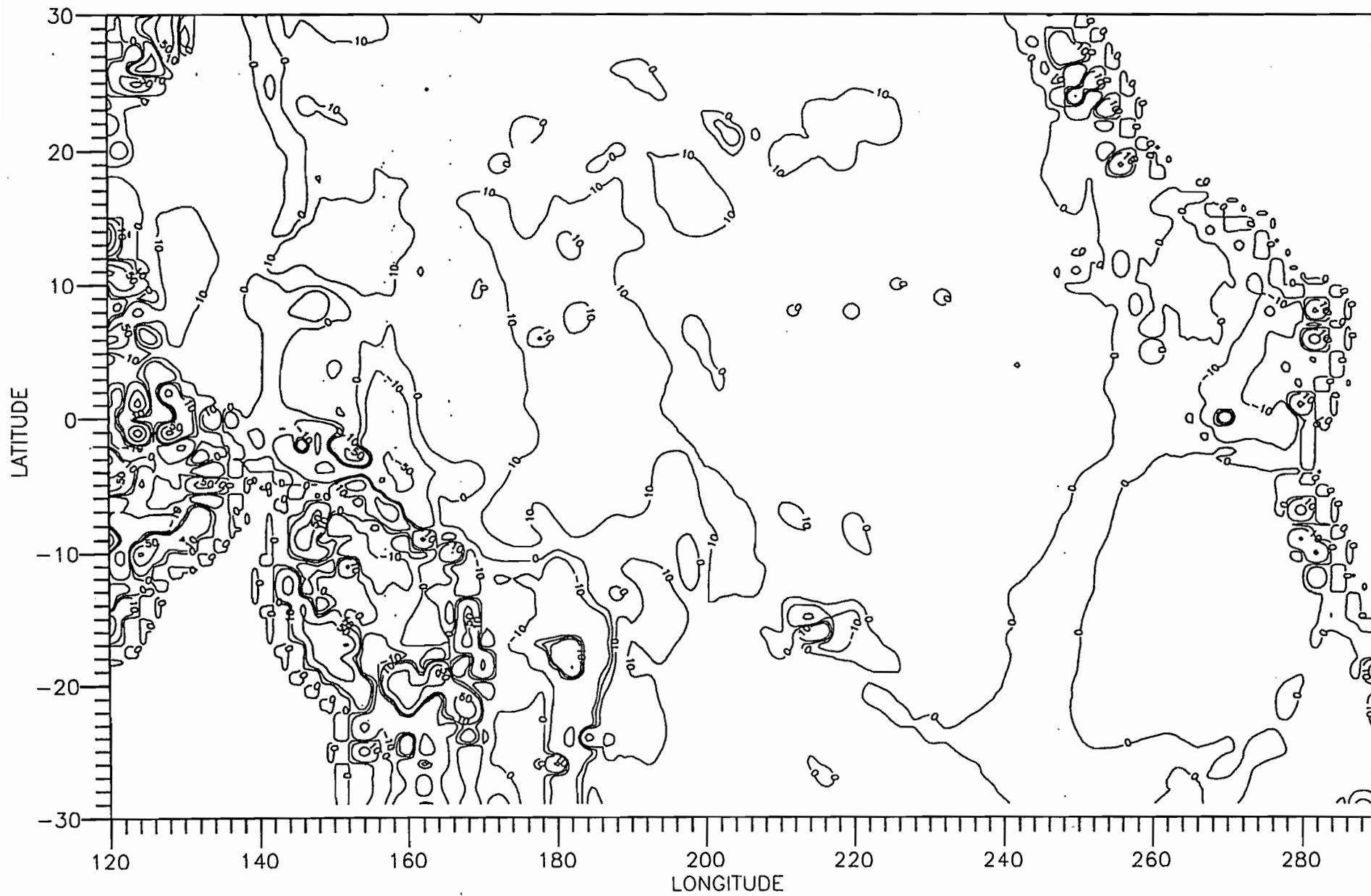
FIG.24 Contour plot of the differences in phase speed (cm/s) for mode 2 when real and mean depths are used.

MODE 3 DIFFERENCES (between real and flat bottom)
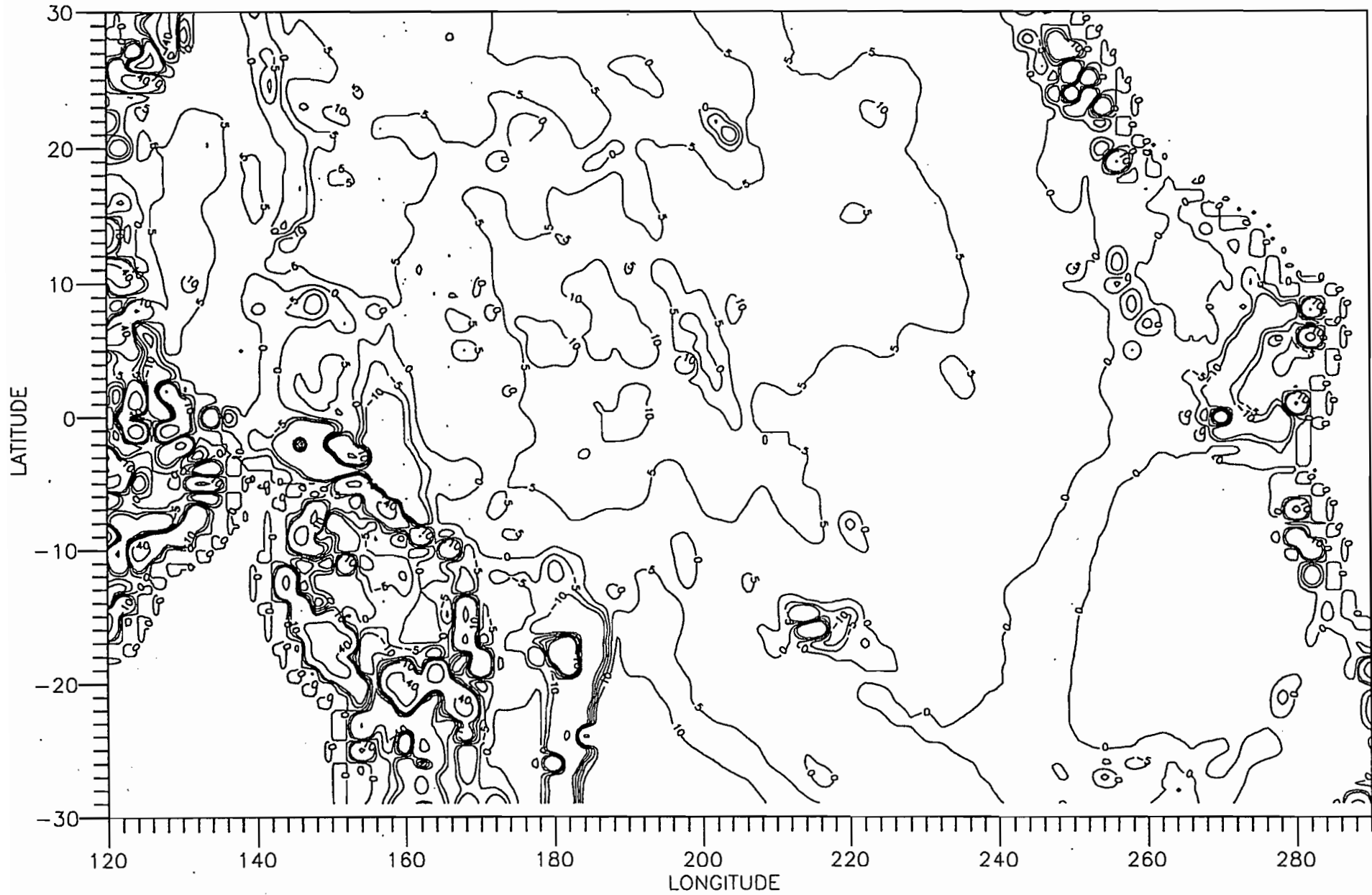
FIG.25. Contour plot of the differences in phase speed (cm/s) in mode 3 when real and mean depths are used.

MODE 4 DIFFERENCES (between real and flat bottom)
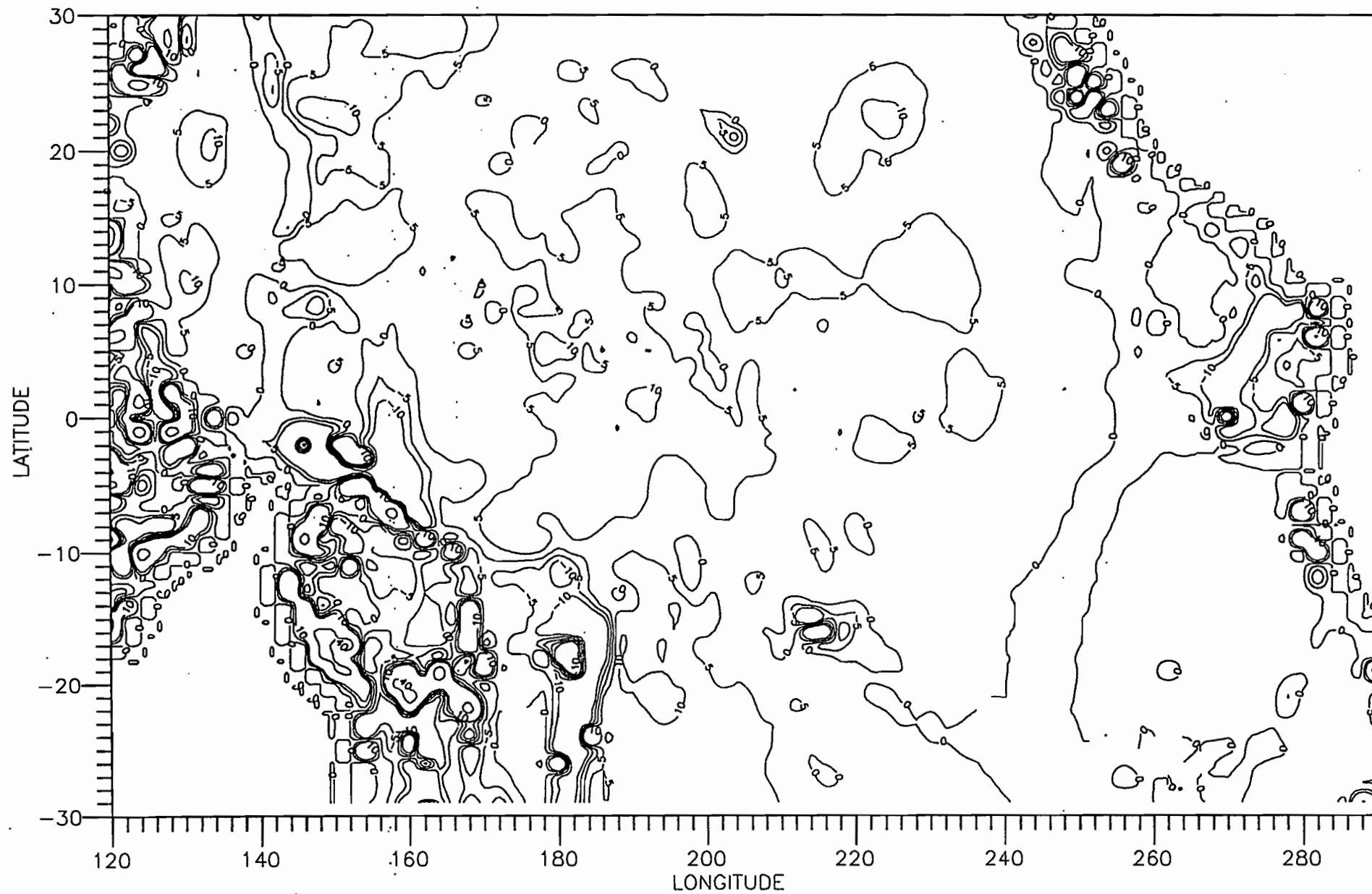
FIG.26:Contour plot of the differences in phase speed (cm/s) for mode 4 when real and mean depths are used.

MODE 5 DIFFERENCES (between real and flat bottom)
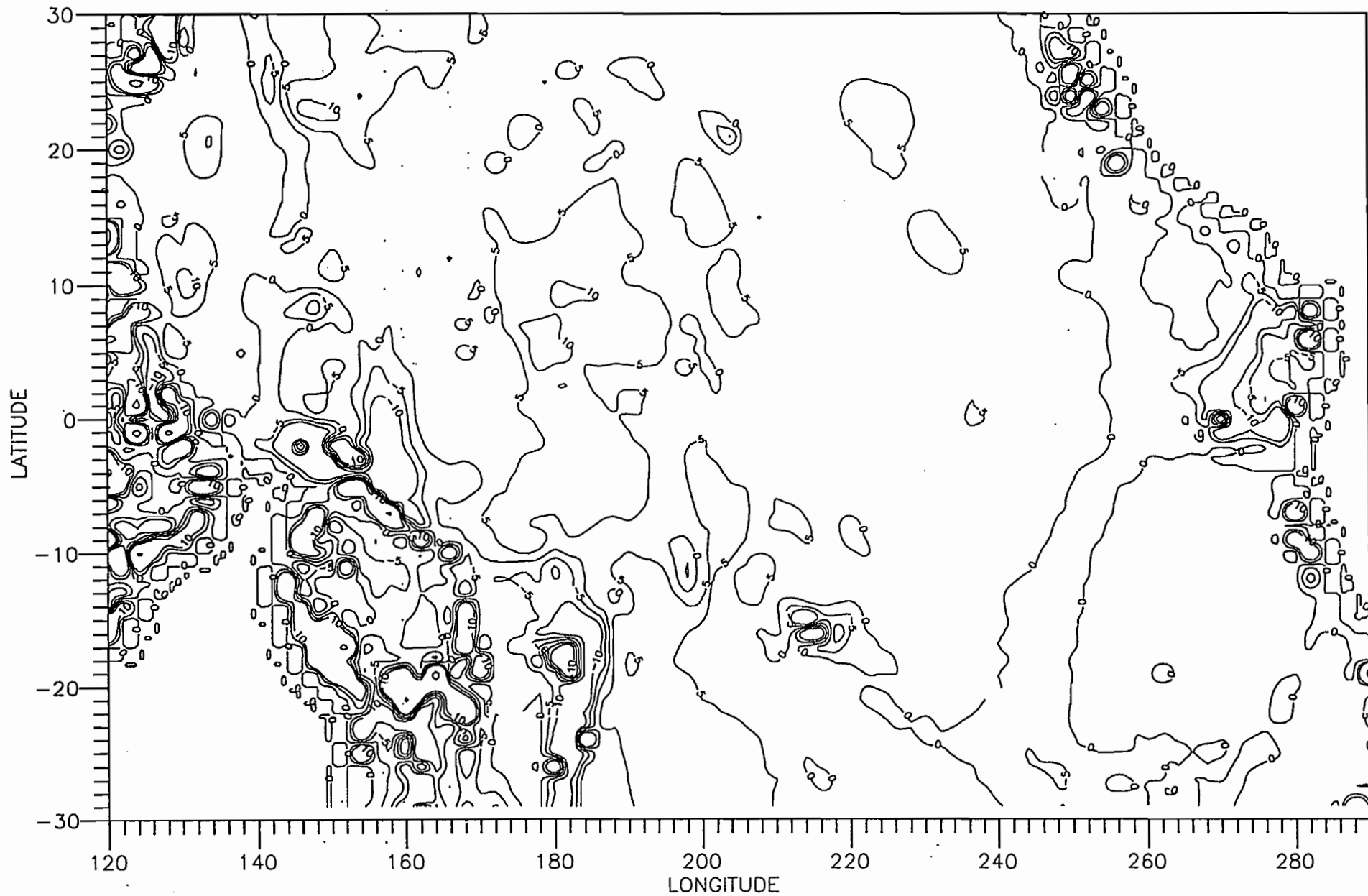
FIG.27.Contour plot of the differences in phase speed (cm/s) for mode 5 when real and mean depths are used.

Corr=0.90

Sig= 0.77e+01

a= 0.80e+00 b= 0.41e+02

npts=4073
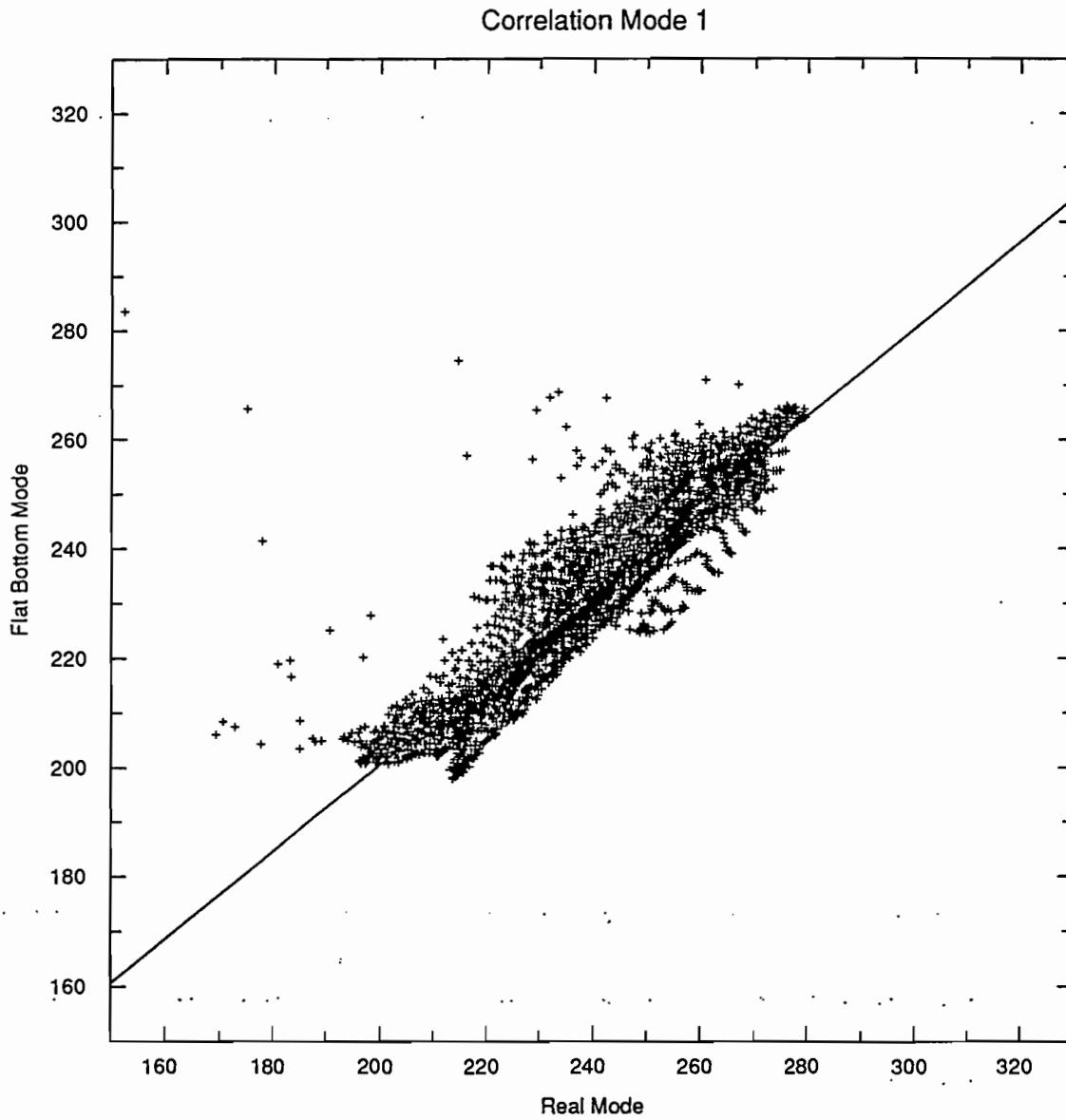
Correlation Mode 1

FIG.28.Correlation between real mode 1 and mode 1 calculated with a flat bottom.

Corr=0.86

Sig= 0.43e+01

a= 0.67e+00 b= 0.40e+02

npts=4073
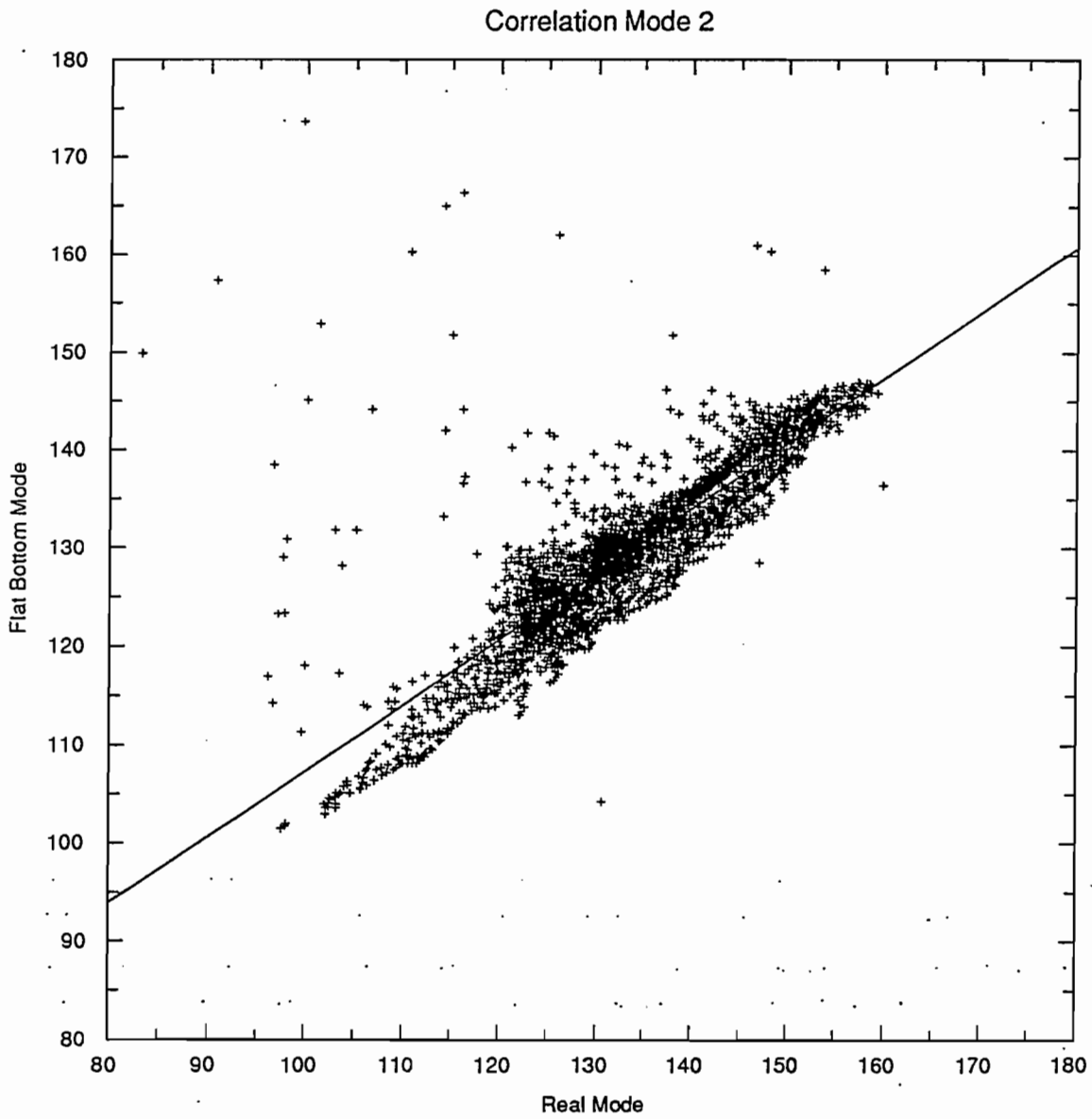
FIG.29.Correlation between real mode 2 and mode 2 calculated with a flat bottom.

Corr=0.71

Sig= 0.34e+01

a= 0.54e+00 b= 0.35e+02

npts=4073
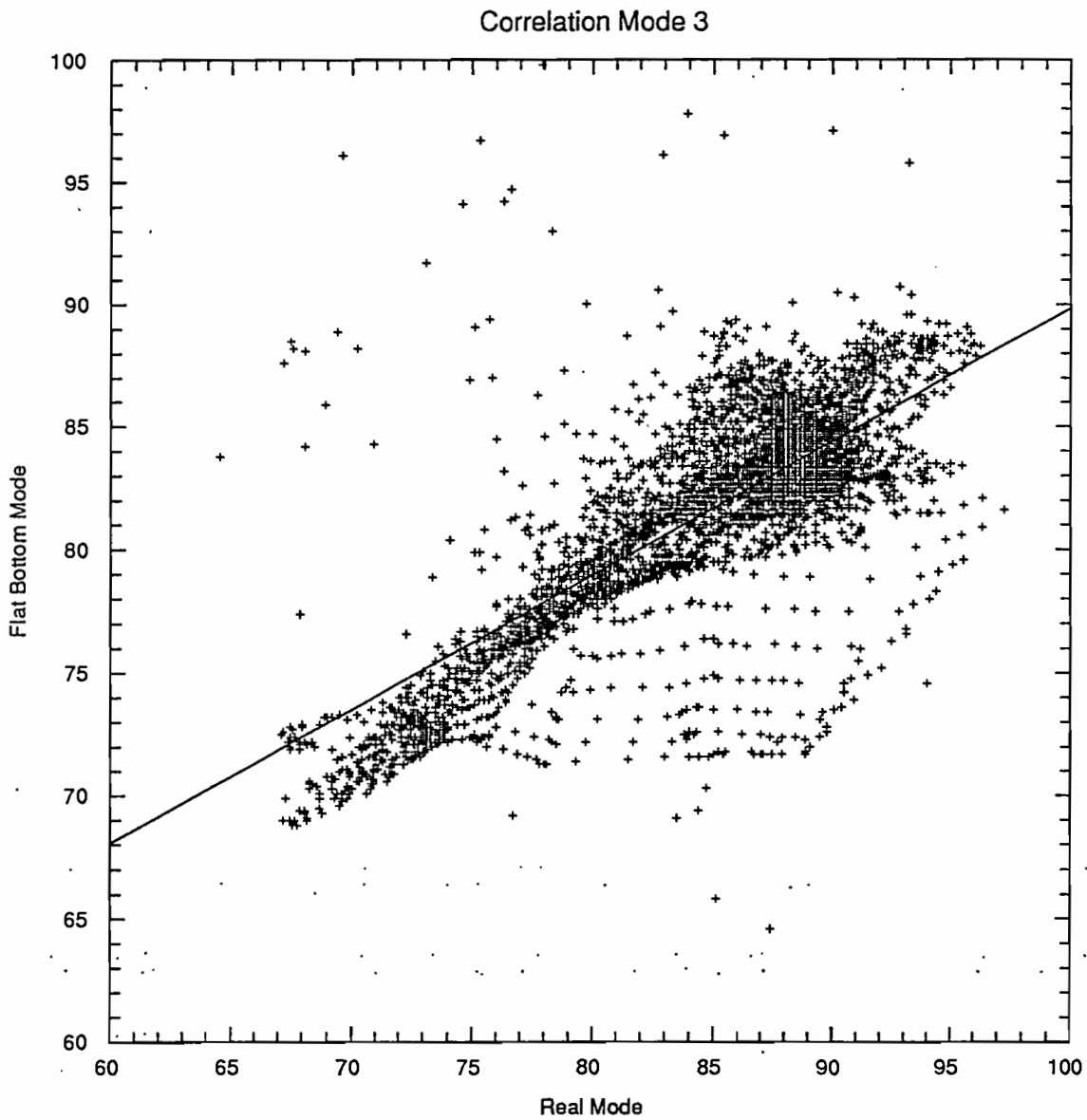
Correlation Mode 3

FIG.30.Correlation between real mode 3 and mode 3 calculated with a flat bottom.

Corr=0.66

Sig= 0.26e+01

a= 0.49e+00 b= 0.29e+02

npts=4073
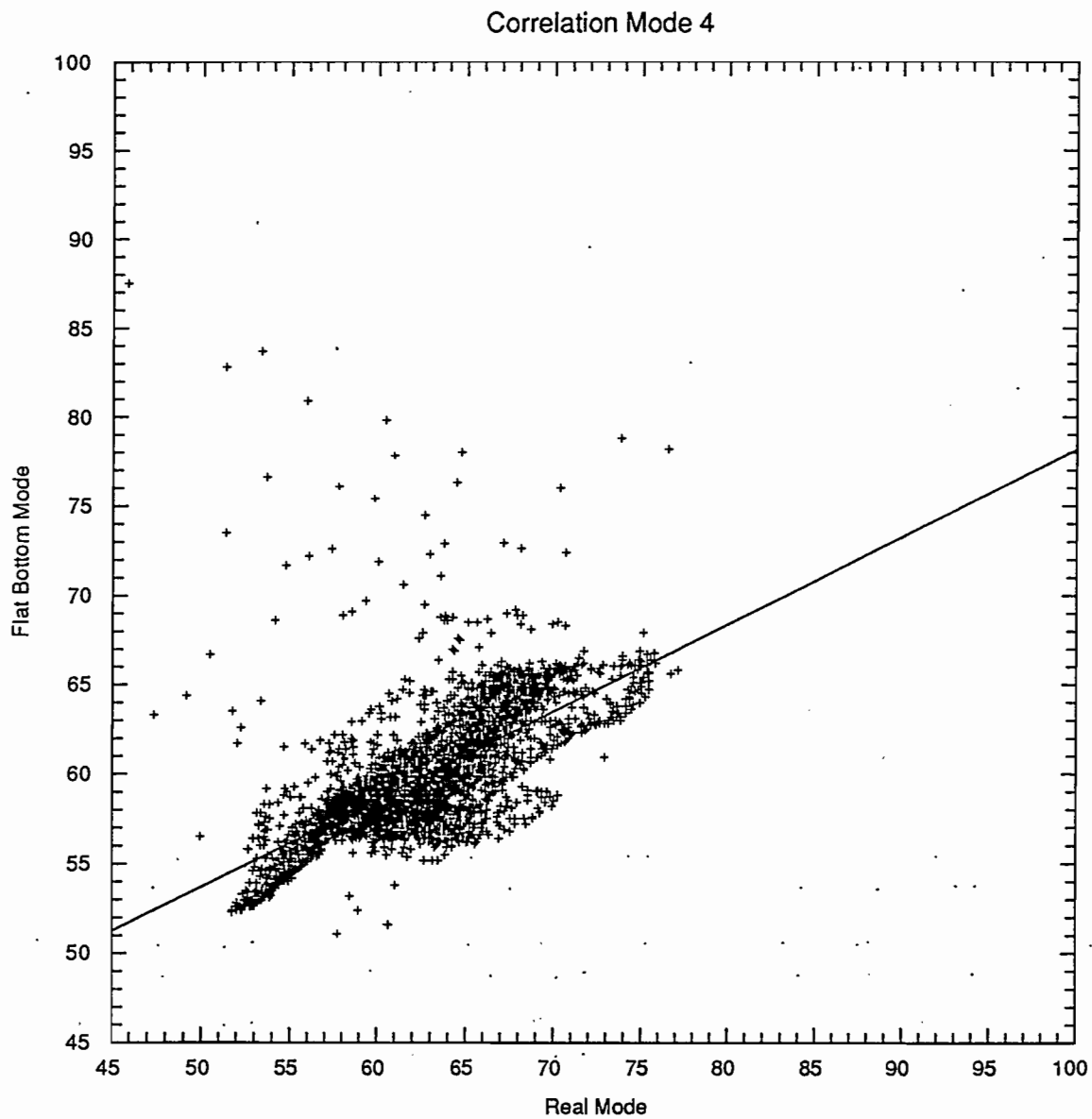
Correlation Mode 4

FIG.31.Correlation between real mode 4 and mode 4 calculated with a flat bottom.

Corr=0.69

Sig= 0.20e+01

a= 0.48e+00 b= 0.24e+02

npts=4073
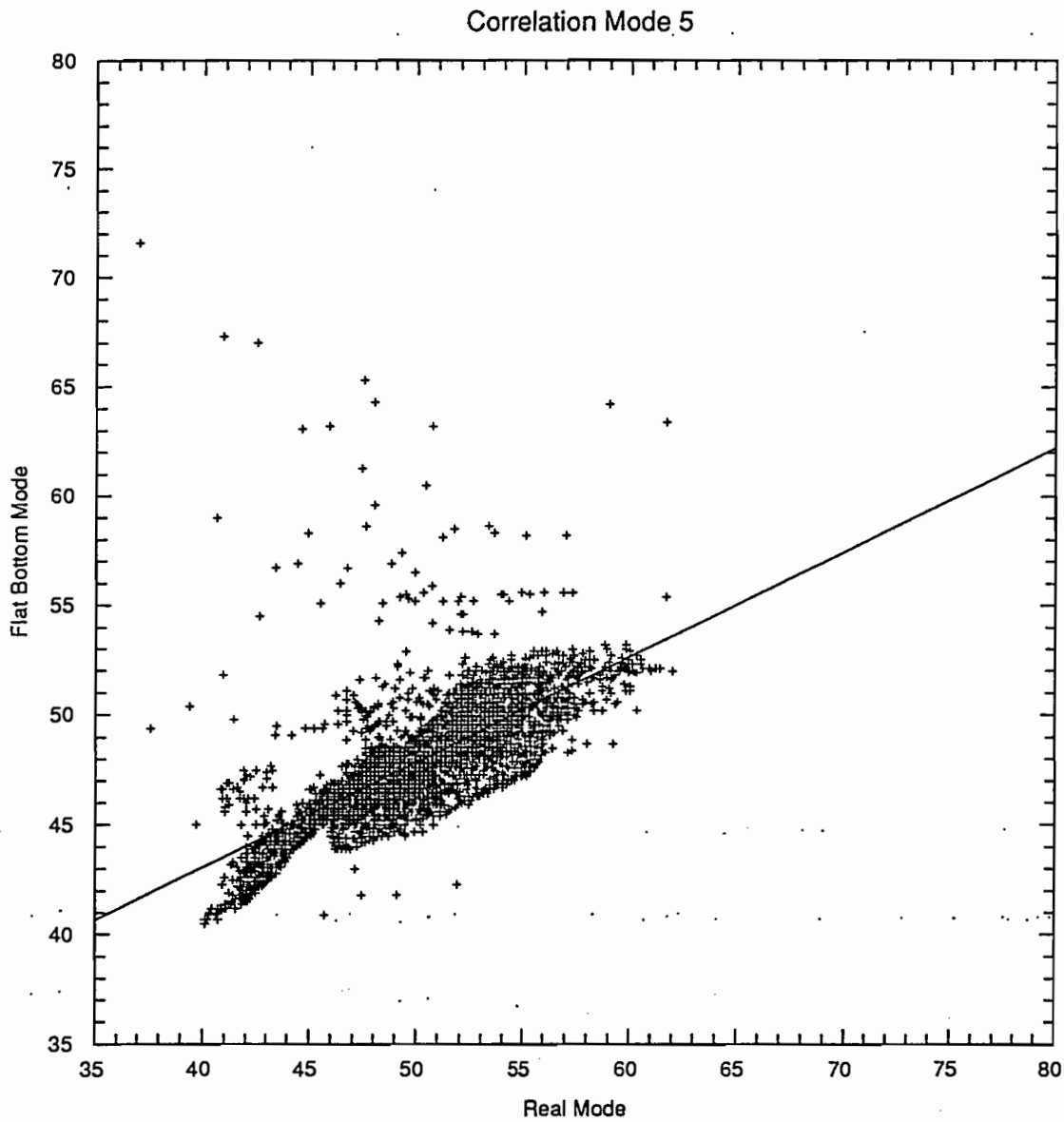
FIG.32.Correlation between real mode 5 and mode 5 calculated with a flat bottom.

Corr=0.53

Sig= 0.21e+01

a= 0.64e-01 b= 0.18e+03

npts=4082
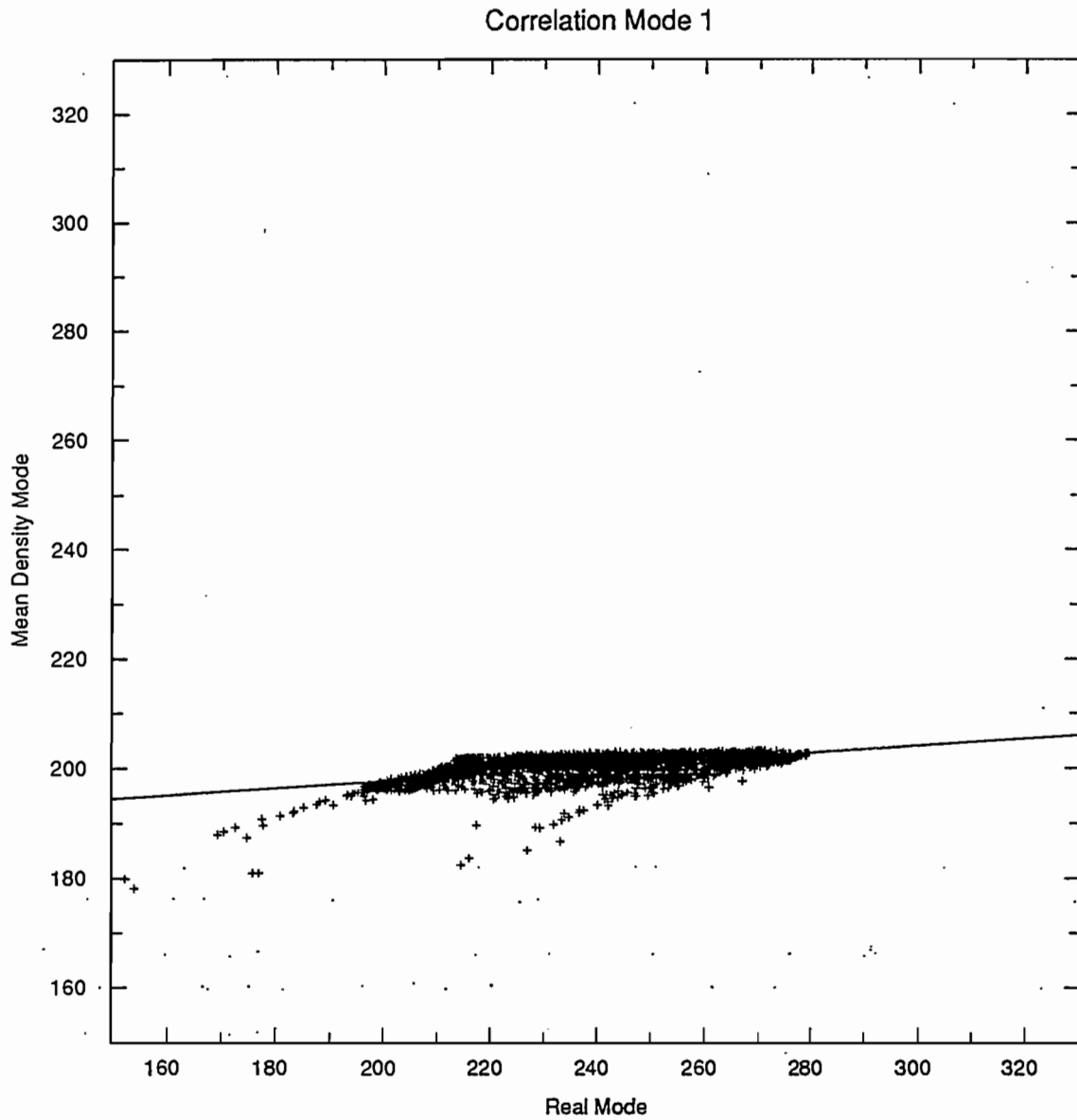
Correlation Mode 1

FIG.33.Correlation between real mode 1 and mode 1 calculated with a mean density profile.

Corr=0.68

Sig= 0.55e+00

a= 0.47e-01 b= 0.84e+02

npts=4082
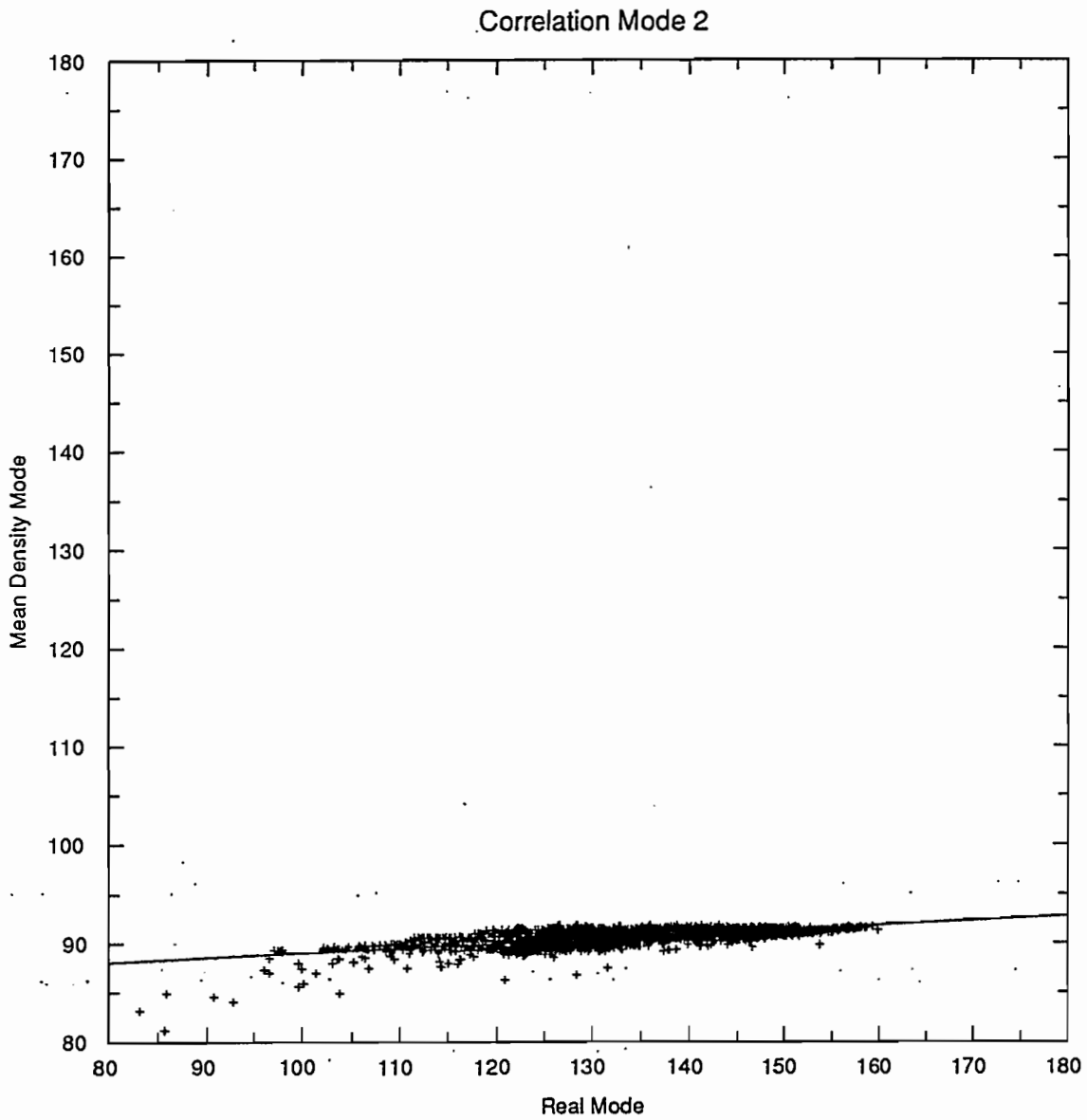
FIG.34.Correlation between real mode 2 and mode 2 calculated with a mean density profile.

Corr=0.77

Sig= 0.41e+00

a= 0.79e-01 b= 0.49e+02

npts=4082
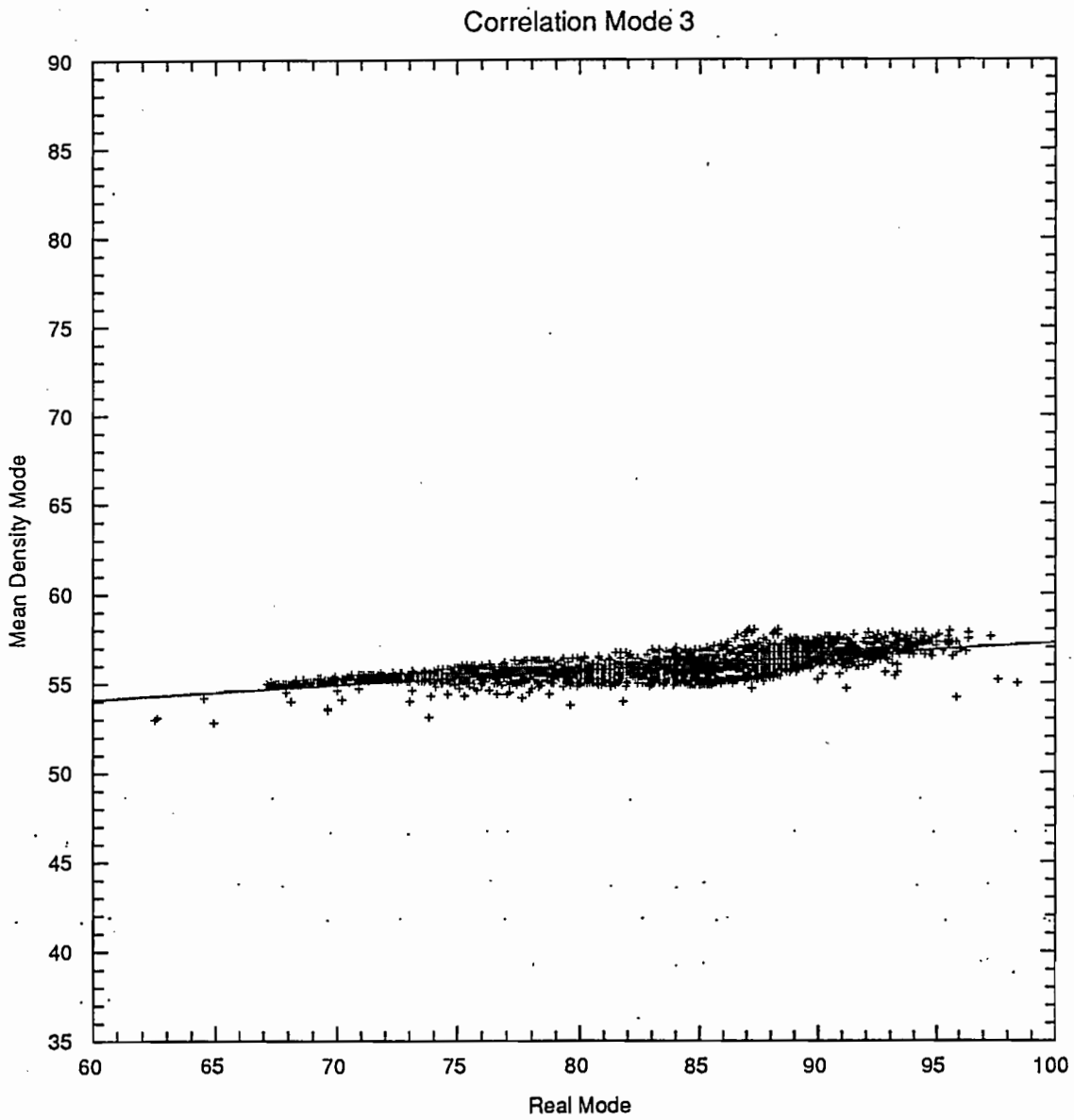
FIG.35.Correlation between real mode 3 and mode 3 calculated with a mean density profile.

Corr=0.71

Sig= 0.13e+01

a= 0.28e+00 b= 0.25e+02

npts=4082
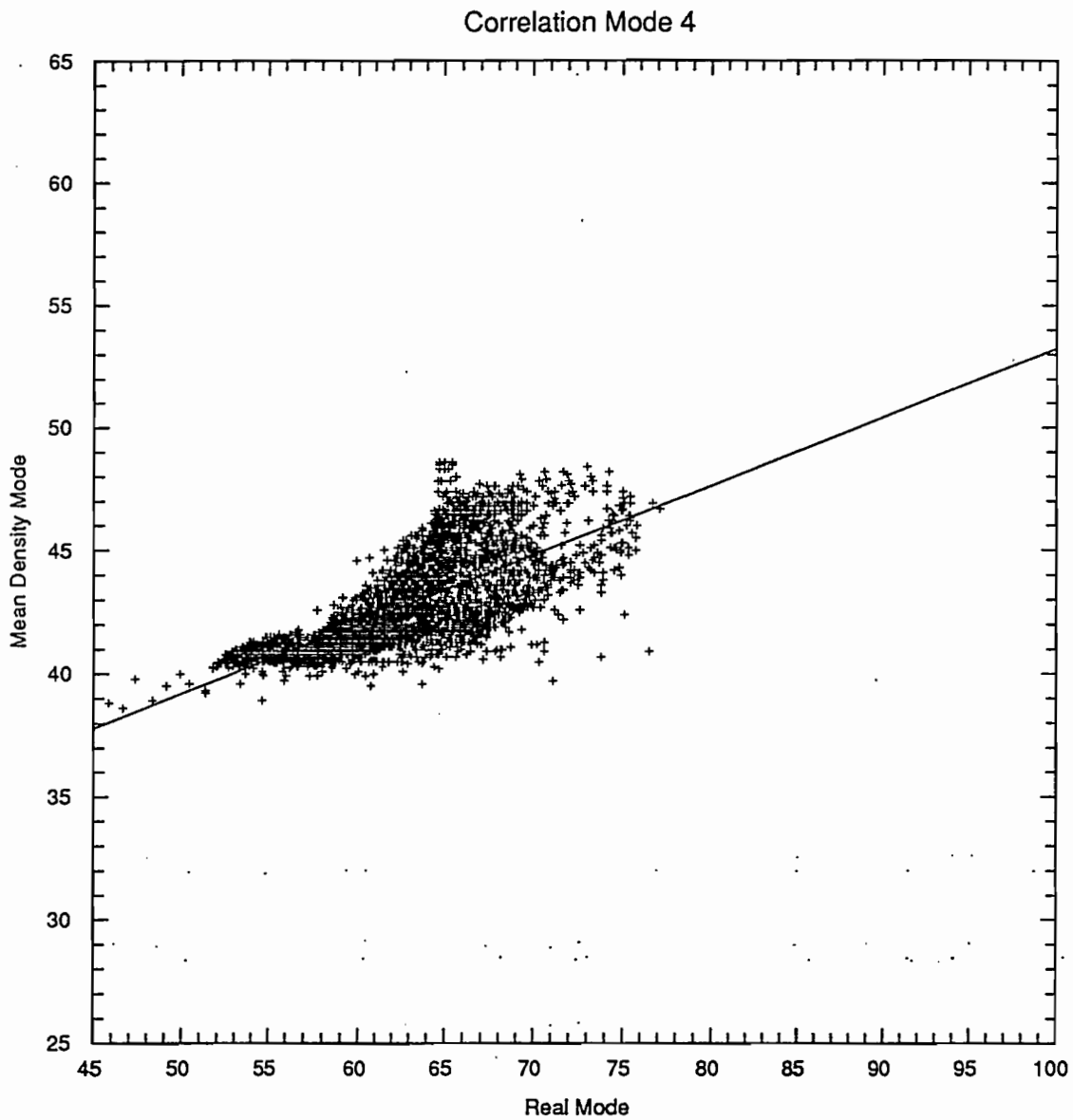
FIG.36.Correlation between real mode 4 and mode 4 calculated with a mean density profile.

Corr=0.79

Sig= 0.13e+01

a= 0.41e+00 b= 0.15e+02

npts=4082
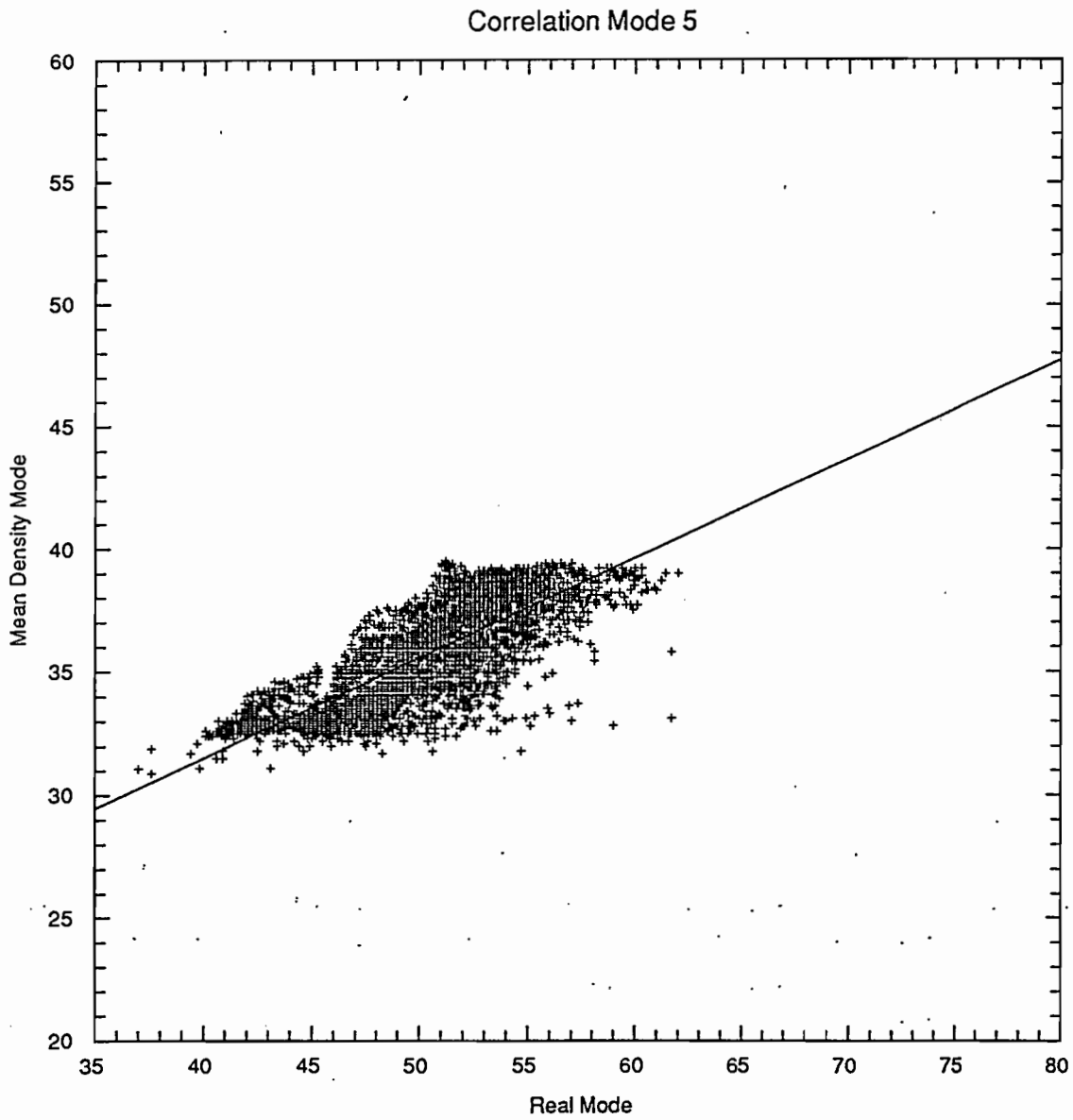
FIG.37.Correlation between real mode 5 and mode 5 calculated with a mean density profile.

LAT   10.5 LON   200.5   (Levitus file)

C = 232.8 147.4 88.8 64.0 52.8
An(0) = .5.08 5.18 2.39 2.74 2.71

C = 241.7 150.1 91.8 65.1 53.9
An(0) = 4.82 5.38 2.38 2.62 2.83
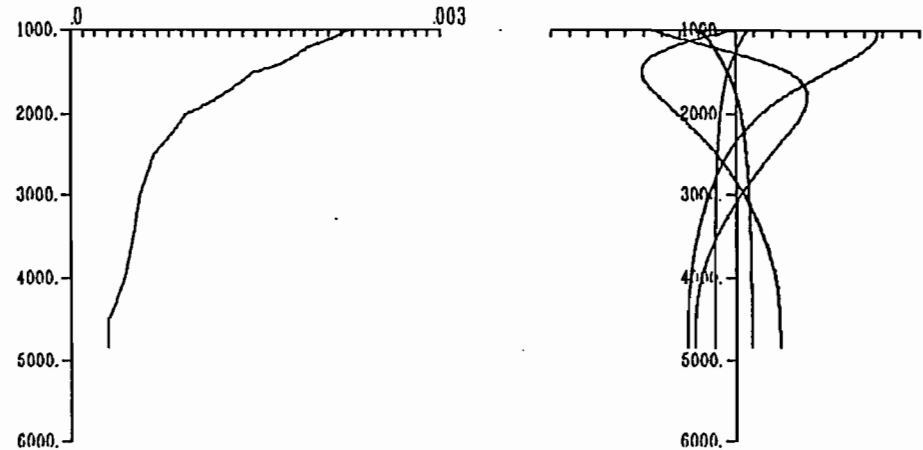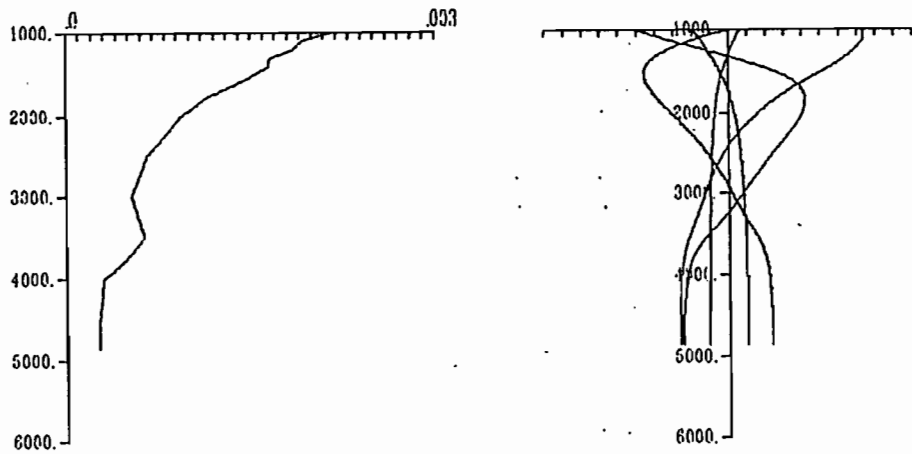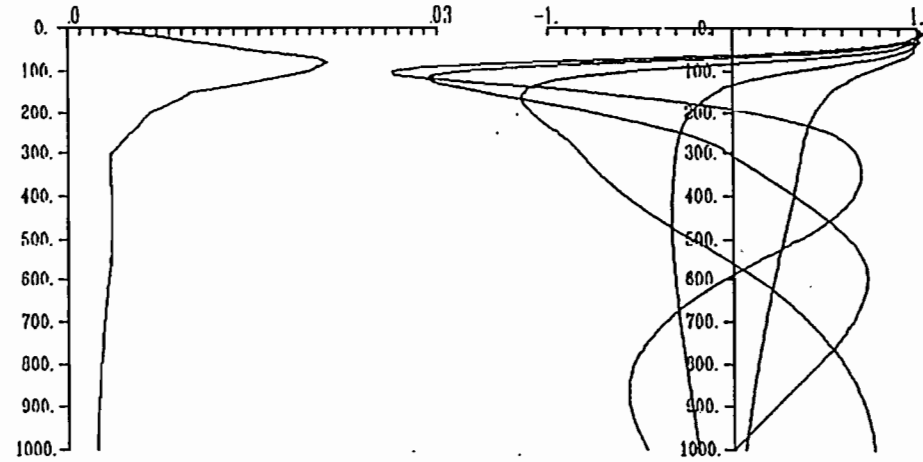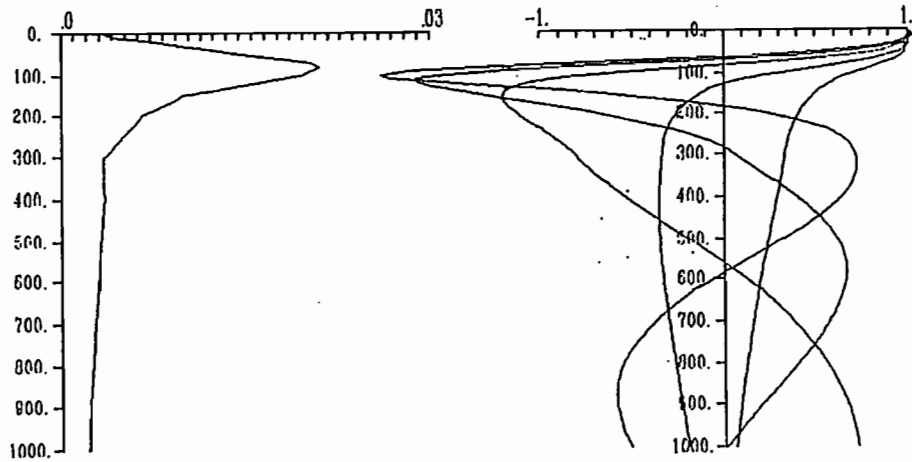
VAISALA FREQUENCY   MODES
(REAL)

VAISALA FREQUENCY   MODES
(CONNECTED)

FIG.38.Comparison of the real modal structure (left) and the modal structure obtained with the
connected Väisäla profile (right) for the position 10.5 N, 160.5 W.

C = 269.3 150.0 91.8 68.4 54.0
An(0) = 4.88 3.23 2.82 2.60 2.45

C = 275.9 155.9 94.1 70.8 56.4
An(0) = 4.73 3.40 2.72 2.60 2.32
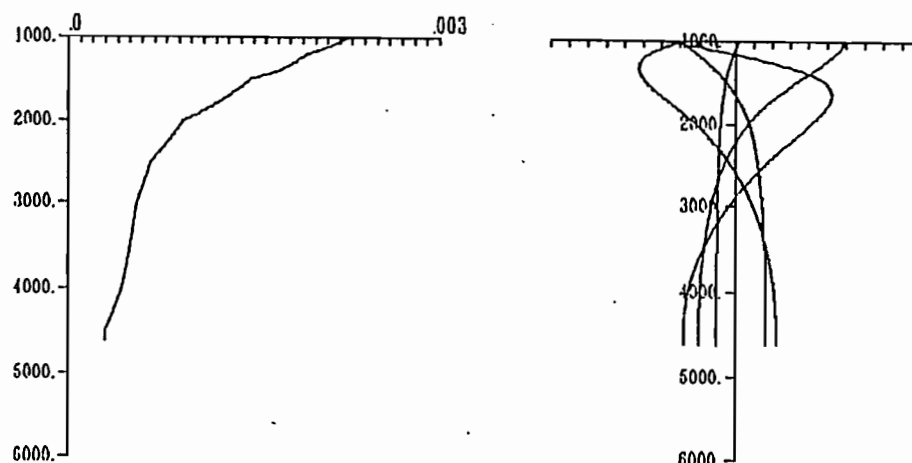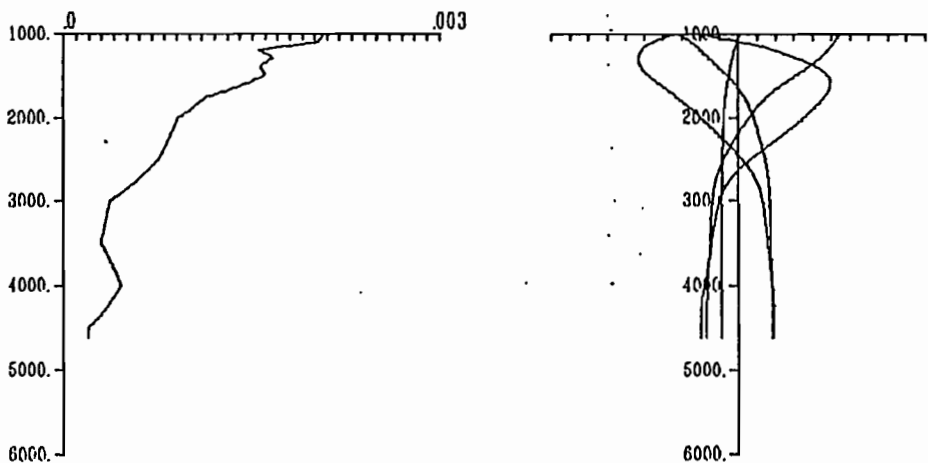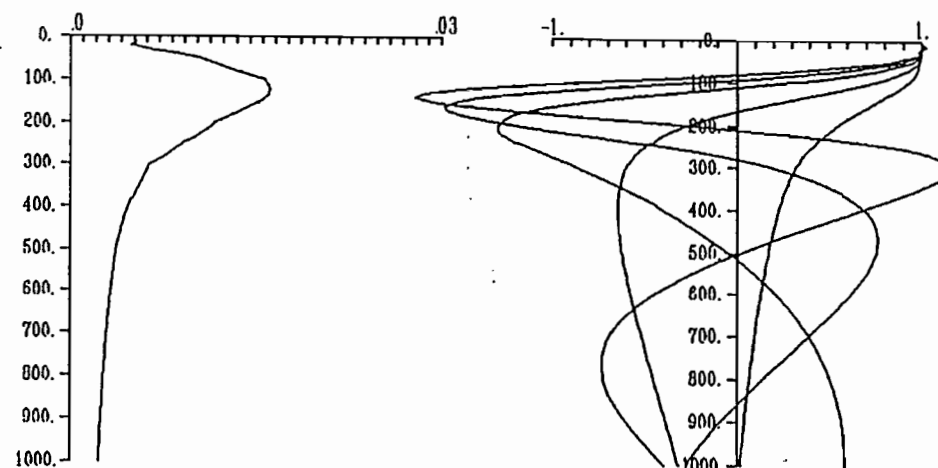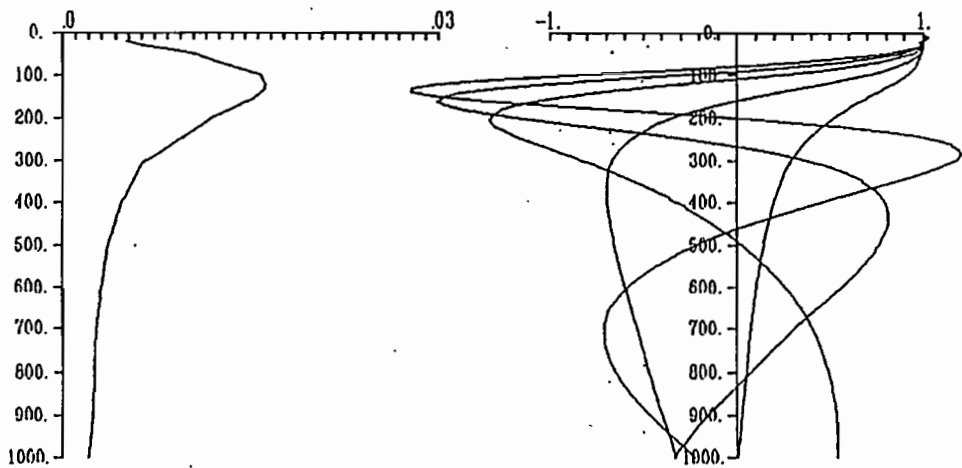
VAISALA FREQUENCY
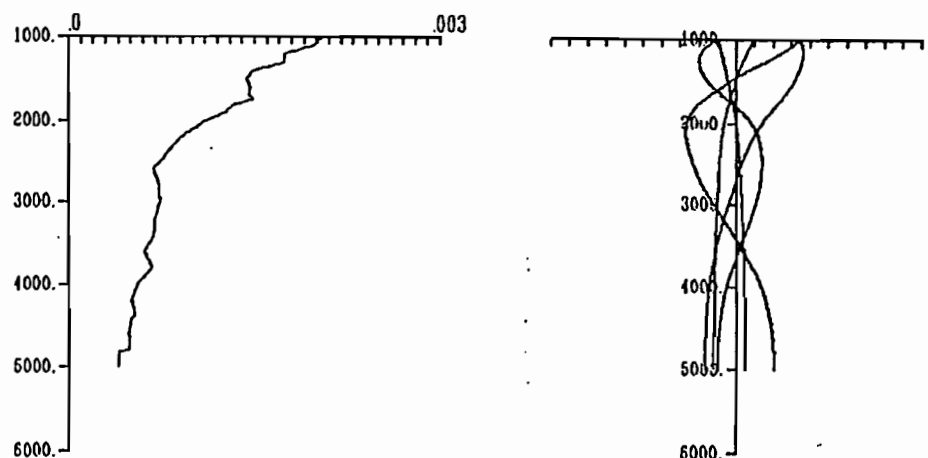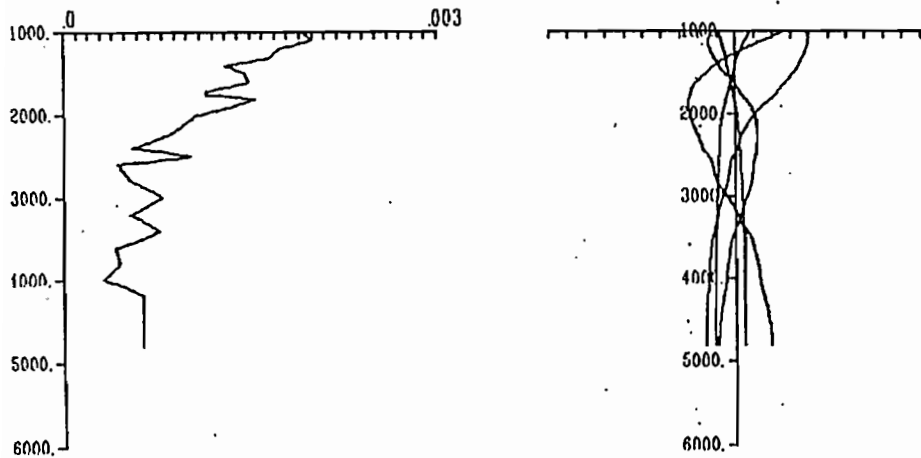(REAL)

MODES

VAISALA FREQUENCY
(CONNECTED)

MODES

FIG.39.Comparison of the real modal structure (left) and the modal structure obtained with the connected Väisälä profile (right) for the position 12.5 N, 138.5 E.

LAT   8.5 LON   150.5   (Levitus file)

C = 242.5 146.2   83.4   65.3   51.5
An(0) = 4.79   2.93   2.35   2.28   1.86

C = 250.1 151.3   86.6   66.5   51.6
An(0) = 4.60   3.21   2.15   2.50   1.84

VAISALA FREQUENCY
(REAL)

MODES

VAISALA FREQUENCY
(CONNECTED)

MODES

54
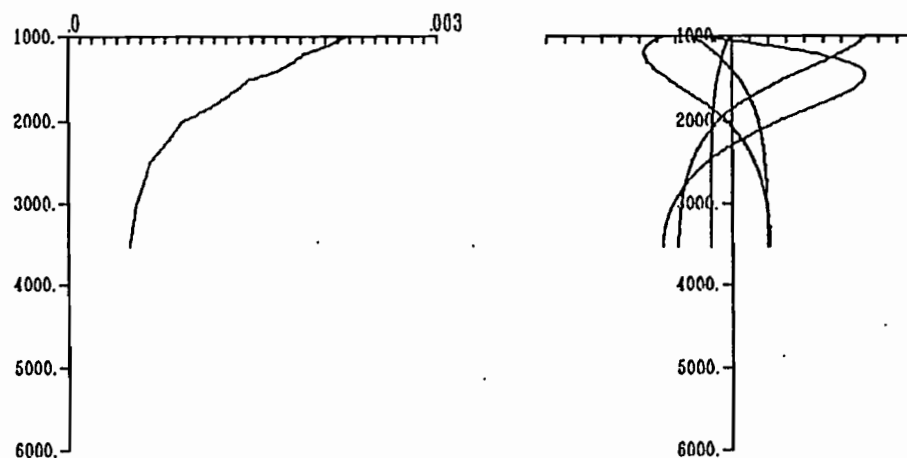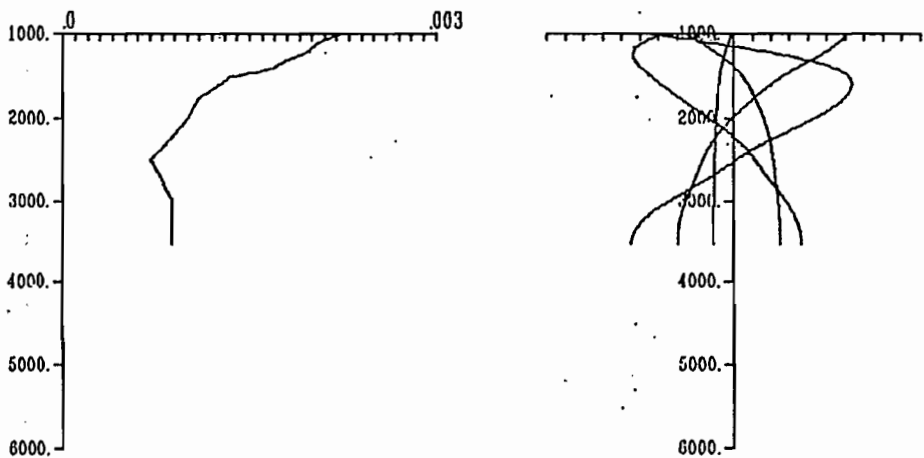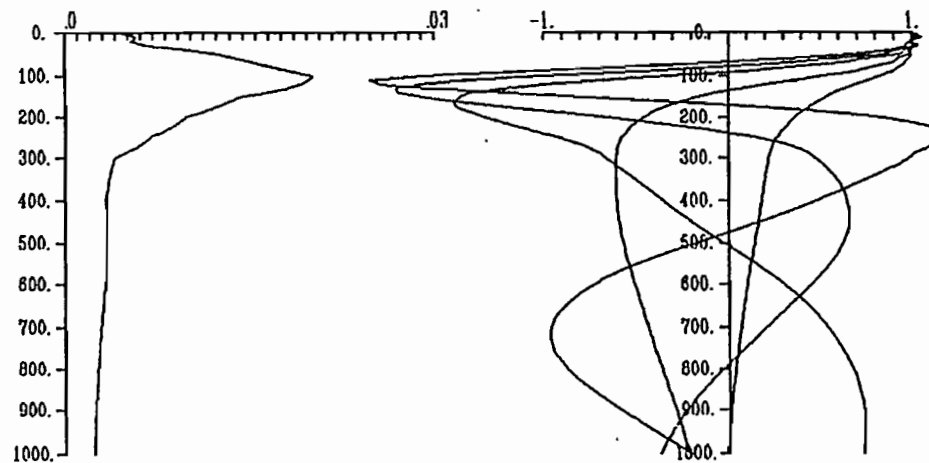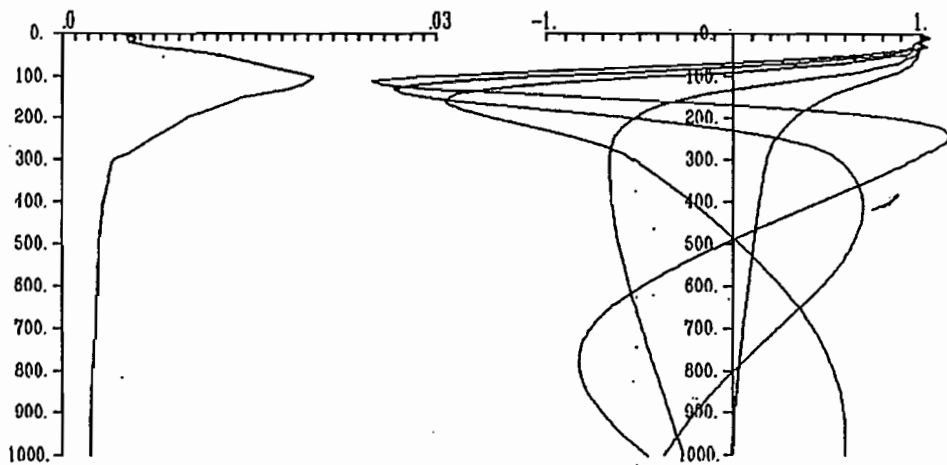
FIG.40.Comparison of the real modal structure (left) and the modal structure obtained with the
connected Väisäla profile (right) for the position 8.5 N, 150.5 E.

C = 214.6 116.1   86.5   62.5   50.0
An(0) = 3.52 6.92 5.87 2.92 3.15

C = 217.7 117.2   89.2   65.0   51.1
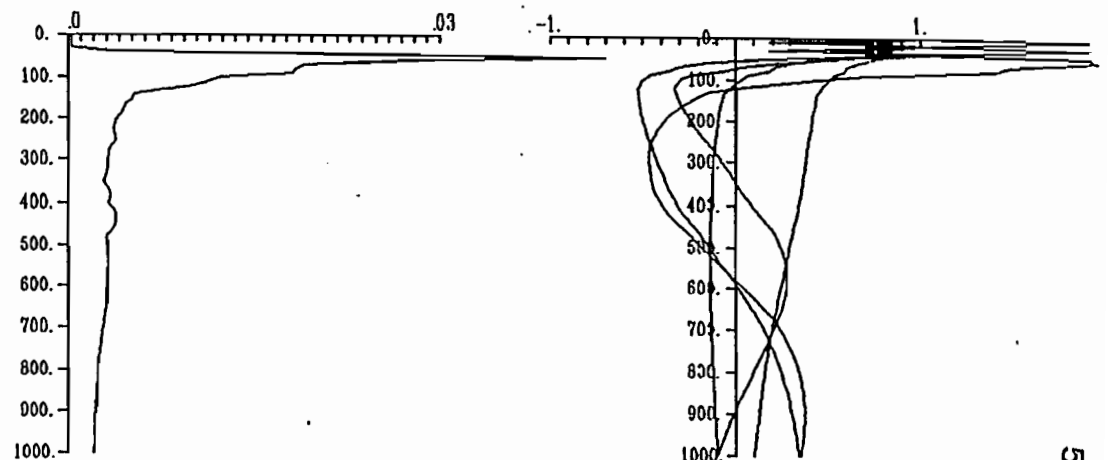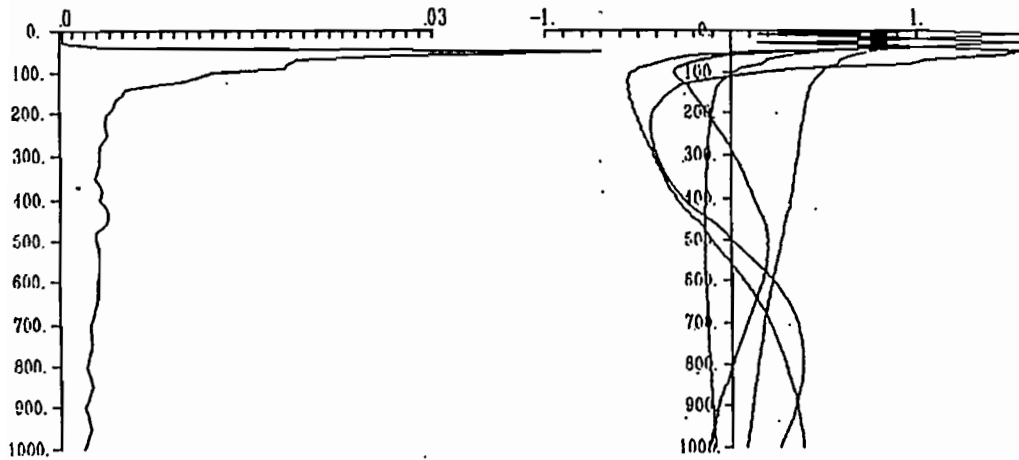An(0) = 3.59 6.75 6.20 3.01 3.32

55

VAISALA FREQUENCY

(REAL)

MODES

VAISALA FREQUENCY

(CONNECTED)

MODES
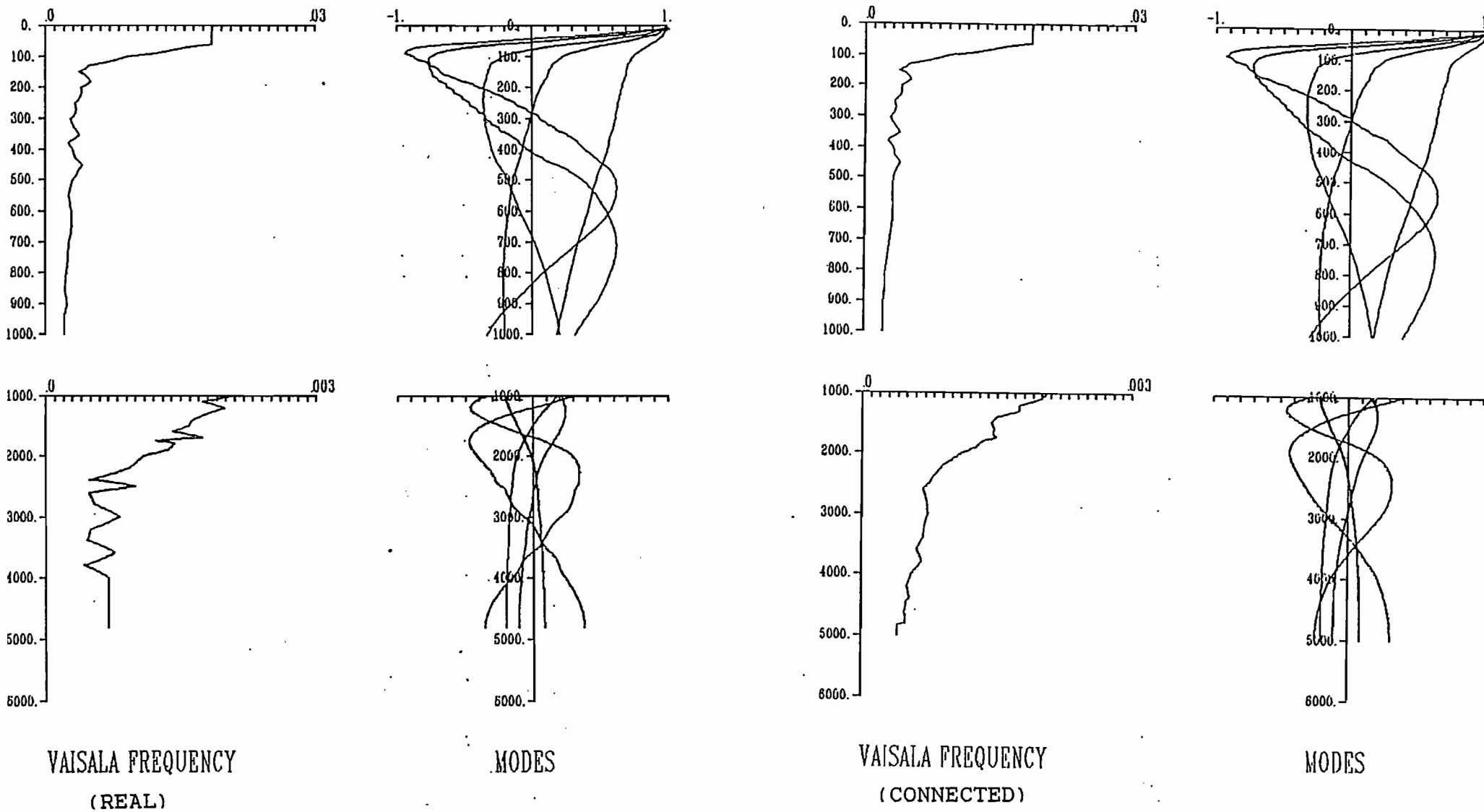
FIG.41.Comparison of the real modal structure (left) and the modal structure obtained with the connected Väisäla profile (right) for the position 8.27 N, 150.54 W.

LAT 8.265 LON 150.162   (NODC file)

C = 219.4 142.7 93.9 57.5 48.0
An(0) = 5.56 9.40 4.24 3.85 8.12

C = 224.7 144.8 97.7 59.8 49.8
An(0) = 5.41 9.63 4.46 3.35 6.64
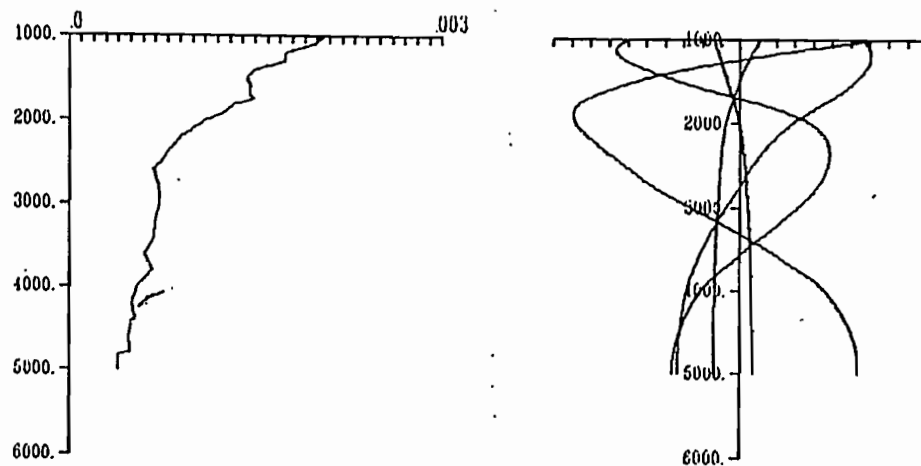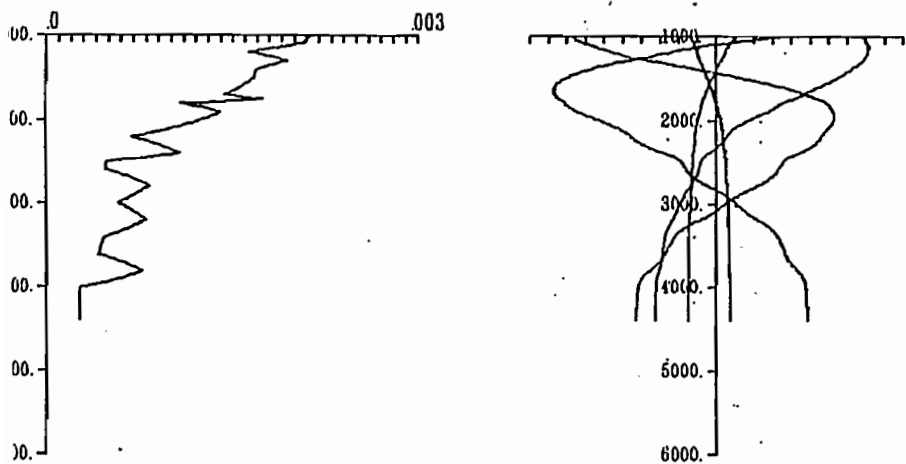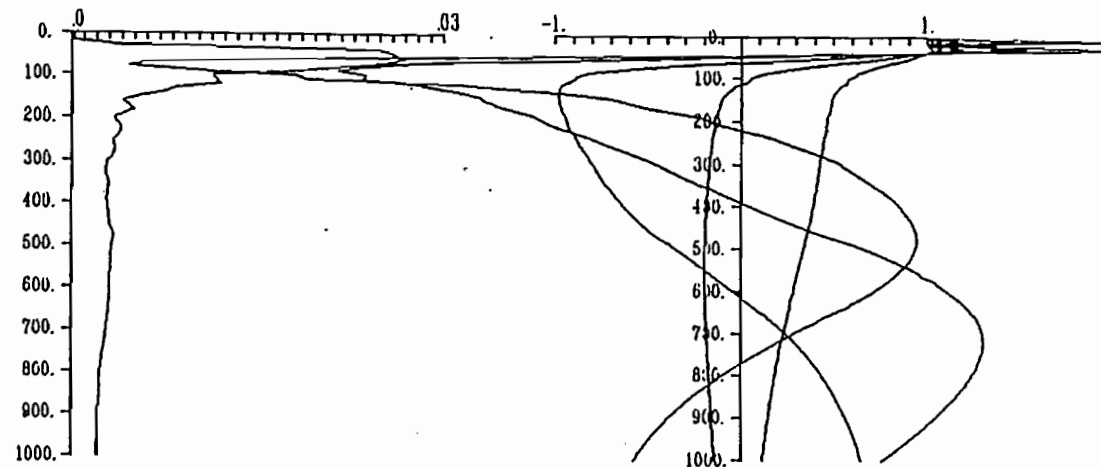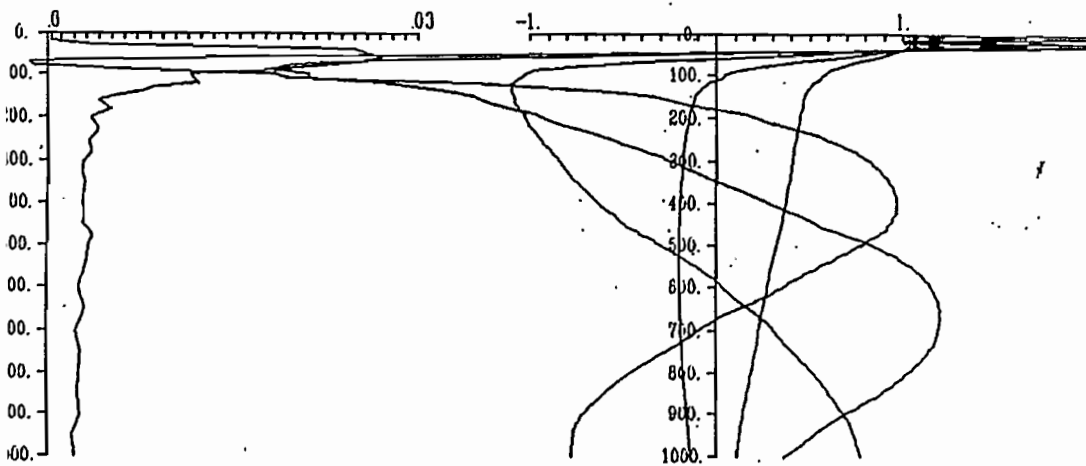
VAISALA FREQUENCY
(REAL)

MODES

VAISALA FREQUENCY
(CONNECTED)

MODES

FIG.43. Comparison of the real modal structure (left) and the modal structure obtained with the connected Väisäla profile (right) for the position 8.26 N, 150.16 W.

LAT 7.597° LON 150.427 (NODC file)

C = 219.7 143.7 91.1 61.8 50.9
An(0) = 4.48 6.53 2.11 1.57 1.64

C = 223.7 144.4 95.9 65.6 53.3
An(0) = 4.69 6.97 2.35 1.46 1.88

57

VAISALA FREQUENCY

(REAL)

MODES

VAISALA FREQUENCY

(CONNECTED)

MODES

FIG.42.Comparison of the real modal structure (left) and the modal structure obtained with the connected Väisäla profile (right) for the position 7.60 N, 150.43 W.